

**POLYMER PARTICLE INTERACTIONS
IN NANOCOLLOIDS**

by

BURCU OZEL

Submitted to the Graduate School of Engineering and Natural Sciences

in partial fulfillment of

the requirements for the degree of

Master of Science

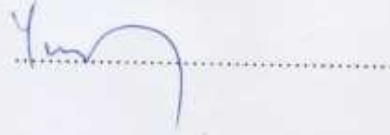
Sabanci University

August, 2011

POLYMER PARTICLE INTERACTIONS
IN NANOCOLLOIDS

APPROVED BY:

Yusuf Mencelođlu
(Thesis Supervisor)



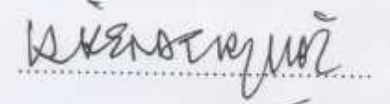
Mehmet Yıldız
(Thesis Co-Supervisor)



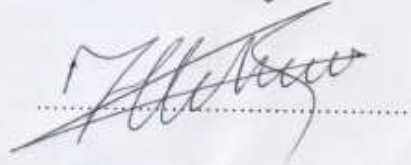
Canan Atılgan



İskender Yılgör



Fevzi akmak Cebeci



DATE OF APPROVAL: 16/08/11

© Burcu ÖZEL 2011

All Rights Reserved

POLYMER PARTICLE INTERACTIONS IN NANOCOLLOIDS

Burcu ÖZEL

MAT, Master's Thesis, 2011

Thesis Supervisor: Yusuf Ziya Menceloğlu, Mehmet Yıldız

**Keyword: Colloids, Hydrophobic/philic Surface, Non-Newtonian Flow,
Interparticle Interaction**

ABSTRACT

The rheological properties of complex fluids has been one of the interesting research subject due to the macroscopic behaviour (namely shear thinning and shear thickening) exhibited when they are subject to shear force. All concentrated suspensions under right conditions can exhibit the non-Newtonian flow behaviour, however, the required conditions and the underlying mechanism are not well understood in literature. To this respect, this study systematically investigates the effects of physicochemical parameters on the flow behavior of colloidal nanoparticle suspension (CNS) to shed a light on the mechanism behind the shear thickening behavior of CNS. We have also presented the outcomes of experimental studies of CNS with a low particle volume fraction, and anisotropic and flocculated microstructures through measuring their viscosity and electrical resistance under various shear forces together with utilizing several relevant characterization methods (i.e., Dynamic Light Scattering, Transmission Electron Microscopy and Capacitance Measurement). It is observed that studied CNS display shear thickening/thinning flow behavior depending on their microstructure forms due to the interaction forces among particles and associated changes in floc sizes, which are controlled by the shear induced hydrodynamical forces. The detailed evaluation of the experimental results indicates that the shear thickening phenomena in low volume fraction, anisotropic and flocculated systems is mainly attributed to the increase in the total surface area and the effective volume fraction of particles due to both hydrodynamic and interparticle forces.

NANOKOLLOİDLERDE POLİMER PARÇACIK ETKİLEŞİMLERİ

Burcu ÖZEL

MAT, Master Tezi, 2011

Tez Danışmanı: Yusuf Ziya Menceloğlu, Mehmet Yıldız

**Anahtar Kelimeler: Kolloidler, Hidrofobik/filik Yüzey, Newtonsal Olmayan Akış,
Parçacıklar Arası Etkileşim**

ÖZET

Kompleks akışkanların kayma kuvvetlerine maruz bırakıldıklarında göstermiş oldukları kayma kalınlaşması ve kayma incilmesi gibi reolojik özellikler ilgi çekici araştırma konularından bir tanesidir. Bütün yoğunlaştırılmış süspansiyonlar doğru koşullar altında Newtonsal olmayan akış davranışı gösterebilmektedirler fakat uygun koşullar ve ardında yatan mekanizma literatürde tam olarak anlaşılammıştır. Bu nedenle, çalışma kapsamında süspansiyonların kayma kalınlaşması davranışına ışık tutabilmek için fizikokimyasal parametrelerin nanoparçacık içeren kolloidal süspansiyonların akış davranışına olan etkileri sistematik olarak incelenmiştir. Ayrıca düşük parçacık hacim fraksiyonuna sahip, anisotropik ve topaklanmış parçacıklardan oluşan sistemlerin deneysel sonuçları çeşitli karakterizasyon teknikleri (Ör., Dinamik Işık Saçılımı, Geçirimli Elektron Mikroskopi ve Kapasitans Ölçümleri) ile birlikte viskozite ve elektiriksel direnç ölçümlerinin çıktısı olarak sunulmuştur. Süspansiyonların, parçacıklar arası etkileşimlerden dolayı meydana gelen mikroyapılara ve hidrodinamik kuvvetlerin kontrolü ile bu yapıların büyüklüğünde meydana gelen değişime bağlı olarak kayma kalınlaşması/incilmesi akış davranışı gösterebildiği gözlemlenmiştir. Düşük parçacık hacim fraksiyonuna sahip, anisotropik ve topaklanmış parçacıklardan oluşan sistemlerin kayma kalınlaşması davranışı göstermesi, yapılan deneysel çalışma çıktılarının detaylı incelenmesi sonucunda hidrodinamik ve parçacıklar arası etkileşim kuvvetlerinden ötürü parçacıkların yüzey alanının ve efektif hacim fraksiyonunun artmasına bağlı olduğu belirtilmiştir.

To my father and mother
Alaaddin & Nuran GENÇ

ACKNOWLEDGMENTS

I would like to express my gratitude to all those who gave me the possibility to complete the thesis. First of all, I would like to thank to my advisor, Yusuf Ziya Mencelođlu, for his patience and guidance throughout this research and for his generosity for sharing his experiences with me and invaluable support. Also, I would like to give my special thanks to my co-advisor Mehmet Yıldız for his patient guidance, encouragement and excellent advises throughout the research. Moreover, I am grateful to have a chance to work with my advisor and co-advisor.

I also would like to thank my colleagues Elif Özden Yenigün, Sinem Taş, Firuze Okyay, Özlem Kocabaş, Yeliz Ekinci, Kaan Bilge, Eren Şimşek, Erim Ülkümen, Mustafa Baysal, Ayça Abakay, Gülcan Çorapçiođlu, Melike Mercan Yıldızhan, Güliz İnan, Shauti Shalima, Tuğçe Akkaş, Burcu Saner, Özge Malay, İbrahim İnanç, Kinyas Aydın, Murat Gökhan Eskin, Hasan Kurt, Gönül Kulođlu for patience, friendship and support at Sabancı University. Many thanks go in particular to my professor in Sabancı University for their encouragement and their valuable comments and suggestions.

The funding provided by The Scientific and Technological Research Council of Turkey (TUBITAK) under the support program of scientific and technological research projects (1001) for the 110M202 numbered project is gratefully acknowledged. I would like to thank Prof. Meric Ozcan of Sabancı University, Faculty of Engineering and Natural Sciences for his technical assistance on the electrical resistance measurement experiments in this research.

I am also thankful to my colleagues at Bosch Siemens Home Appliances for their support.

Finally, I would like to thank to my beloved parents and husband; Alaaddin, Nuran GENÇ, Nalan, Özgür LALE, Alime, Kemal GEZER, Banu GENÇ, Serdar, Nevin ÖZEL and Seçkin ÖZEL for their endless love, patience and encouragement during all stages of my life.

TABLE OF CONTENTS

1. INTRODUCTION	1
2. LITERATURE REVIEW	4
3. EXPERIMENTAL	10
3.1. Materials	10
3.2. Characterizations	11
4. RESULT AND DISCUSSIONS	14
4.1. Chemical Parameters	15
4.1.1. Monomeric fluids: Effect of hydrogen bonding interactions	17
4.1.2. Polymeric fluids: Influence of interparticle interactions	21
4.1.2.1. Steady shear rheological analysis	22
4.1.2.1.1. Shear thickening mechanism	24
4.1.2.1.2. Hydrodynamic effect	26
4.1.2.1.3. Effect of interparticle interactions	30
4.1.2.2. Oscillatory shear rheological analysis	38
4.2. Physical Parameters	50
5. CONCLUSION	55
APPENDIX	57
REFERENCES	59

LIST OF FIGURES

Figure 3.1. Schematic representations of (a) primary flow units (aggregate) and agglomerate structures of fumed silica, (b) the hydrophilic fumed silica (N20) which contains hydroxyl functional groups on the surface and the hydrophobic fumed silica (H15) with both hydroxyl and methyl groups on the surface.....	10
Figure 3.2. The schematic representation of a parallel plate capacitor (left), and the integration of the rheometer with the digital multimeter for the electrical resistance measurements (right).....	13
Figure 4.1. Steady rheological behavior of suspensions in order to understand the effect of hydrogen bonding capability of continuous media.....	16
Figure 4.2. Viscosity versus shear rate profile of suspensions (M3-M6) and polyethylene glycol, ethylene propylene oxide copolymer.....	17
Figure 4.3. Schematic representations for interparticle interactions in dispersions of (a) M3, (b) M4, (c) M5, (d) M6.....	23
Figure 4.4. The electrical resistance measurements of HFSi+Peg+Lithium chloride dispersion under the applied shear during the viscosity analysis, and without the applied shear at the stationary condition.....	25
Figure 4.5. Viscosity and electrical resistance versus time plot of the HFSi+Peg+Lithium chloride mixture and a schematic representation for the microstructural change in a mixture under the shear.....	26
Figure 4.6. A schematic representation for shear thickening in a concentrated, spherical, monodisperse and close packed colloid system, (a) the relative motion of particles at low shear forces, (b) the increase of the viscosity due to the formation of extra void volume at high shear forces.....	29
Figure 4.7. A schematic representation for the shear thickening in a concentrated, anisotropic, polydisperse colloid system, (a) the relative motion of small flocculated particles at low shear forces, (b) the increase of viscosity due to the increase of particle surface area and formation of extra void volume between them at high shear forces.....	29
Figure 4.8. Rotational motion of an anisotropic particle induced by a shear field.....	30

Figure 4.9. Schematic representations for particles with adsorbed layers, (a) a high molecular weight polymer is adsorbed on the particle surface, hence forming a dense polymer layer. This situation generates strong repulsive force, (b) low molecular weight polymer is adsorbed on the particle surface, thus forming a thin adsorbed polymer layer. This situation generates a weak repulsive force, and consequently vdW attractive force might become dominant.....	34
Figure 4.10. Cryo-TEM image of M4.....	36
Figure 4.11. DLS results of the M2 and M4 suspensions.....	37
Figure 4.12. The viscosity versus shear stress profile of the M2 and M4 suspensions.....	38
Figure 4.13. Elastic modulus versus strain profile of M2 and M4 suspensions.....	39
Figure 4.14. Strain sweep experiment under oscillatory shear (a)M3, (b) M4, (c) M5 and (d) M6.....	43
Figure 4.15. Frequency sweep analysis at 0.1 strain amplitude; (a) M3, (b) M4, (c) M5, (d) M6.....	44
Figure 4.16. (a) Complex viscosity of suspensions at frequency 50 rad/s during strain sweep analysis and (b) Complex viscosity of M6 at different frequencies.....	46
Figure 4.17. Single frequency (1.59 hz) oscillator shear experiments (at controlled stress (10 Pa)) (a) M3, (b) M4, (c) M5 and (d) M6.....	48
Figure 4.18. Thixotropic analysis (preshear is applied at 5 Pa); (a) M6, (b) M5, (c) M4 and (d) M3.....	50
Figure 4.19. Steady shear experiment of suspensions composed of different molecular weight polymeric matrix.....	52
Figure 4.20. Minimum and maximum viscosity differences and the critical shear rates for suspensions (M3, M7-M9).....	52
Figure 4.21. Steady shear viscosity profile of suspensions composed of different sizes particles.....	53

Figure 4.22. The effect of particle mass fraction on the non-Newtonian flow behavior.....53

Figure 4.23. Hydrodynamic radius of particles in suspensions measured by dynamic light scattering of suspensions.....54

Figure 4.24. Effect of preprocessing speed on the dispersion and concomitant change of rheology of the suspensions.....54

LIST OF TABLES

Table 3.1. Properties of continuous liquid phase used in this study.....	11
Table 3.2. Formulations of studied suspensions.....	12
Table 4.1. Schematic representations for microstructural changes of suspensions under shear.....	17
Table 4.2. Dielectric constant and refractive index of constituents of suspensions (M1, M2, M3).....	19
Table 4.3. Dielectric constant, refractive index of constituent and the effective Hamaker constant of mixtures. Note that dielectric constants of our particles are compiled from literature.....	33
Table 4.4. Results of quantitative thixotropic analysis.....	50

LIST OF SCHEMA

Schema 4.1. A schema that shows experimental parameters for studied nano colloids.....	15
---	----

LIST OF ABBREVIATIONS

CNS:	Colloidal nanoparticle suspensions
ODT:	Order disorder transition
STF:	Shear thickening fluids
HFSI:	Hydrophilic fumed silica
HPFSI:	Hydrophobic fumed silica
EG:	Ethylene glycol
GLY:	Glycerin
PEG:	Polyethylene glycol
EPO-PPO:	Ethylene-propylene oxide copolymer
TEM:	Transmission electron microscopy
DLS:	Dynamic light scattering
HR:	Hydrodynamic radius
BET:	Brunauer, Emmett and Teller

CHAPTER I

1. INTRODUCTION

The rheological properties of colloidal nanoparticle suspensions (CNS) have been attracting the attention of scientist and engineers for use in many important industrial applications since these fluids exhibit complex non-Newtonian flow behavior (either shear thinning or shear thickening) when subjected to external shear forces. Blood and paints might be listed as common examples of shear thinning materials. Widely used in Li battery technology, the mixture of polymer electrolyte and small size inorganic particles also demonstrates a shear thinning behavior [1,2]. Shear thinning is also a familiar phenomenon in polymer solutions and molten polymers, which facilitates the transport of these type of fluids through processing equipment since the pressure drop at the walls is reduced due to the decrease in the fluid viscosity [3]. Contrary to the shear thinning, the shear thickening phenomenon is not a preferred fluid behavior in certain industrial processes such as polymeric nano-composites manufacturing process since it adversely affects the performance of the process as well as the process-ability of material [4]. Stating otherwise, the shear rate and also the viscosity of shear thickening fluid are maximum at the walls of the processing equipment, thereby causing pressure built-up therein. Nevertheless, the shear thickening behavior of colloidal suspensions can be advantageous for some other specific applications and thus, have resulted in a tremendous amount of industrial and commercial innovations in many areas. For example, shear-thickening fluids can be used for applications such as biomedical, sportswear, damping devices, shock absorbers for automotive industry and ballistic protection, among others [5].

The structural transition from fluid to solid like behavior of shear thickening fluid have accelerated research into these fluids over the last few years. In literature, scientists have published many articles that are related to the theory of shear thickening mechanisms and they especially investigate the effect of the chemical parameters. There have been significant efforts devoted to the understanding of the structural origin of the shear thickening phenomenon. These efforts have led to two commonly accepted theories, namely, the Order-to-Disorder Transition (ODT) and Hydrodynamic Clustering [6-10,12]. The ODT theory primarily proposes that particles in concentrated stabilized monodisperse dispersions are hexagonally packed within the fluid layers due to repulsive interparticle forces at low shear

rates. At higher shear rates, however, the magnitude of shear force becomes larger than interparticle forces. As a result, the order in the particle configuration gets disrupted, thereby causing an increase in particle interactions and in turn a rise in the viscosity of the suspension at a critical shear rate [7,8]. The hydrodynamic clustering theory on the other hand suggests the percolation of repulsively interacting particles due to the hydrodynamic force in concentrated hard sphere systems (i.e., commonly 40wt%) [9,10]. These two well known theories are advocated relying on the results of the light/neutron scattering experiments as well as Stokesian Dynamic simulations for the suspensions of sterically or electrostatically stabilized monodisperse spheres [7, 9,11,12]. It is noted that even though these two theories can explain the shear thickening mechanism in colloidal systems with high volume fraction and non-flocculated particles (formed due to the electrostatic and steric repulsive interactions), they do have difficulties in addressing shear thickening in suspensions with low volume fraction and flocculated particles [4,8,13]. Negi et al. and Osuji et al. reported the existence of shear thickening in attractively interacting colloidal suspensions, and attributed the shear thickening phenomena to the break down of dense fractal clusters and a concomitant increase in the effective volume fraction of particles in the system [14,15]. Although a large body of study has been published on the rheology of colloidal suspensions, given the fact that many different types of colloidal systems can be formed, it can be quite challenging to develop a single theory capable of addressing all aspects of the shear thickening mechanism for every suspension. Consequently, the driving forces behind the shear thickening behavior of complex fluids have not been fully understood yet and have remained an ongoing controversial issue in the relevant literature. On the other hand, engineers focus on the applications based on shear thickening fluids hence they examine the physical parameters and their effect on the performance of the final product. Therefore, it is obvious that the control parameters and the underlying mechanism of shear thickening behavior are not well understood because of the lack of detailed and systematical study which investigates both chemical and physical parameters.

In this regard, this study systematically investigates the effects of physicochemical parameters on the shear thickening behaviour of CNS to shed a light on the mechanism behind the shear thickening behaviour of CNS. In this direction, various physicochemical parameters of CNS were investigated; namely, hydrogen bonding capability of monomeric fluids, the types and the molecular weight of polymeric fluids, mass fraction and size of

particle, preprocessing speed and the colloidal interactions between filler and polymeric liquid. It is known that the rheological behavior of CNS is significantly controlled by interfacial interactions between constituents due to the high surface-to-volume ratio of the nanometer size particles. Hence, in addressing the mechanisms behind the non-Newtonian flow behavior in CNS, the colloidal science and the rheology should be considered intimately together since the colloidal science may answer the questions of why the surface chemistry and interparticle forces play important roles in the colloid rheology. Towards this end, we have here attempted to reveal how interparticle interactions result in the formations of various micro structures in colloidal systems and consequently what influences these micro structures have on the non-Newtonian flow behavior. To do so, we have measured the viscosity and the electrical resistance of various suspensions as a function of shear rate/time and time respectively to shed light on their shear thickening mechanism; these suspensions are of low volume fraction, and flocculated structures initially although anisotropic particles are sterically stabilized. The ODT and hydrocluster theory can not be used to interpret the shear thickening response of studied colloids reasonably since they are appropriate for explaining the shear thickening in monodisperse, spherical and high volume fraction systems. Therefore, in light of our experimental results, we propose that the dominant effect for the occurrence of shear thickening phenomenon of the studied suspensions is the decrease in the mobility of polymer chains due to the increase in the total surface area and the effective volume fraction of particles, which are controlled by hydrodynamic effects and interparticle interactions as elaborated in coming sections in detail.

CHAPTER II

2. LITERATURE REVIEW

Nanometer sized inorganic particle filled polymer composites are referred to as colloidal nanoparticle suspensions (CNS) when the polymeric matrix phase is liquid. These filled polymeric systems in melt or in solution are very common and widely used in many industrial applications, ranging from cement mixing to the manufacture of cosmetics and filled polymers [16]. It is known that nano colloids offer improved physical and mechanical properties (i.e., strength, modulus, and heat-distortion temp) in comparison to neat polymers due to the fine particle size and the high surface area of dispersed phase and the interfacial interactions among constituents. On the other hand, CNSs exhibit complex rheological behavior which is rather different from the rheology of neat polymers owing to the addition of inorganic fillers to a polymer matrix. To be more specific, CNSs in general exhibit non-Newtonian (either shear thinning or shear thickening) and viscoelastic behavior unlike the matrix phase which usually possesses a Newtonian character [16]. Shear thinning is defined as a decrease of viscosity with increasing shear rate. Despite being less common, the opposite effect known as the shear thickening can also be observed in various kinds of fluids. In this regard, understanding and subsequently controlling the microstructure and flow properties of CNSs are of vital importance for their processability. Numerous researchers have investigated the rheological behavior of filled systems and reported their steady state shear and oscillatory shear flow properties [17-34]. Shear thickening is often observed in highly concentrated colloidal dispersions, characterized by significant increase in the viscosity with increasing shear rate [5]. The viscosity profile of a shear thickening fluid is highly dependent on the particle volume fraction. In the rheology profile, two Newtonian flow regions are separated by shear thinning flow region at low particle volume fractions. Fluid viscosity does not change at low shear rates, later on shear thinning regime emerges and flow shows again Newtonian profile at higher shear rates. When particle concentration exceeds a critical value, the shear thickening zone appears at high shear rates after a shear thinning regime. The critical shear rate, where the thickening behavior is first observed, shifts to lower values with increasing particle volume fraction. At sufficiently high particle volume fraction, the critical shear rate is such a low value that thinning regime disappears and the viscosity experiences a sudden jump to higher values.

As for the structural origin of the shear thickening, there are two different well known theories; namely, the hydrodynamic clustering and order-to-disorder transition [35]. These theories are supported by previous experimental and simulation studies. Hoffman has provided a direct evidence for structural changes in suspensions under shear through light diffraction experiments which confirm the order-disorder transition [7]. The diffraction pattern suggests that particles are hexagonally packed within the layers and their order disappears after the onset of shear thickening. According to this theory, shear thinning is observed at lower shear rates because of gliding of hexagonally packed particles over each other layer by layer. At a critical shear rate, flow instabilities cause particles to break out of their ordered layer. The disordered structure requires more energy to flow thereby leading to an increase in viscosity, which is referred to as a shear thickening behavior. In other word, the disruption of an ordered structure increases interactions among particles, and hence raises the viscosity of the suspension. However, this theory might not be applicable for explaining the shear thickening behavior of polydisperse and irregular particle suspensions because it is hard to develop layered structures during the flow when particles are not monodisperse and spherical. Laun et al. are the first researches who have questioned the validity of this approach [11]. The hydrodynamic clustering theory states that at very high shear rates, hydrodynamic forces drive particles into contact whereby compact groups of particles are formed. Bossis et al. has utilized Stokesian dynamics simulation to explain flow induced hydrodynamic clustering mechanism in the suspension of spherical Brownian particles [12]. On the other hand, the shear thickening nature of flocculated systems is not predicted by these two well known theories. Osuji et al. have explained the origin of the shear thickening in flocculated systems through the breakup of locally dense clusters of the fractal colloidal particles into less dense structures [15].

Shear thickening phenomenon depends on several physicochemical parameters such as volume fraction, particle shape and size, interparticle interaction, among others, which have been investigated to certain extent in different works. Bertrand et al. showed that the rheological behavior of colloidal suspensions is highly dependent on particle *volume fraction* [21]. Their examination of a suspension composed of bismuth oxychloride (BiOCl) and poly (sodium acrylate) solution indicates that the suspension is a Newtonian liquid at very low volume fraction. At moderate volume fractions, the rheological behavior of the suspension is shear thinning at low shear rates, then shear thickening at higher shear rates and shear

thinning again at the highest accessible shear rates. They also indicate that all these rheological behaviors of suspensions are perfectly reversible. Other important parameters are particle *shape* and *size*. Lootens et al. investigated the rheological behavior of concentrated suspensions of silica particles with controlled roughness [36]. At high enough volume fraction, the viscosity of suspension increases abruptly when a critical shear rate is reached. This transition from low viscosity fluid to a solid like material at a particular shear rate is called as the jamming transitions. They indicated that higher surface roughness of silica particles decreases the shear rate at which jamming transition occurs. One of the very few studies, where the effect of shape has been investigated systematically, is reported by Wetzel et al. [37]. Experiments of Wetzel et al. demonstrated that increasing the particle aspect ratio of ellipsoidal CaCO_3 particles gives rise to a decrease in particle volume fraction at which discontinuous shear thickening behavior can be observed. The nature of the interactions between particles and the continuous media is also another important parameter. Harzallah et al. investigated the rheology of suspensions of hydrophilic/hydrophobic TiO_2 in high molecular weight polyisobutylene in decalin and low molecular weight polybutene in decalin for the application of paints, cosmetics and texture manufacturing [38]. The low molecular weight polybutene (in decalin) shows Newtonian behavior whereas the high molecular weight polyisobutylene (in decalin) indicates shear thinning behavior. When the hydrophilic particles are dispersed in low molecular weight polybutene (PB) solution (in decalin), the suspension shows Newtonian flow behavior. However, the suspension of hydrophobic particles in the same fluid with same volume fraction shows shear thinning behavior and also its zero shear viscosity is higher than the former one. When the hydrophilic/hydrophobic TiO_2 particles dispersed in high molecular weight polyisobutylene (PIB) solution (in decalin) with same volume fraction, the viscosity profiles have the same general behavior; shear thinning. The zero shear viscosity and degree of thinning behavior of the hydrophilic particle in polyisobutylene (PIB) solution is higher than the suspension composed of hydrophobic particles. Raghavan et al. investigated the dispersion of hydrophilic fumed silica in a range of polar organic media [39]. Their results suggested that hydrophilic fumed silica forms stable sols or gels in liquids depending on the hydrogen bonding capability of liquid molecules. According to this hypothesis, particles in stable sols are coated by a solvation layer. This layer forms due to the organization of liquid molecules at the silica interface by forming hydrogen bond with silanol groups present on the silica surface. When the liquid has low hydrogen

bonding capability, particle network forms in the colloid because silica particles are in direct interaction with each other by forming hydrogen bonds with silanol groups. Consequently, the formation of network microstructure causes gelation of suspension. It is clear that the interaction between particles and liquid media determine the flow profile of the suspension.

The applications based on the shear thickening response have attracted a great deal of attention in many areas. For example, fluid filled dampers made of a shear thickening fluid (STF) can be used as seismic protectors for buildings and shock absorbers for automotive industry [40,41]. Additionally, shear thickening fluids lend themselves well to being used in the design of body armor due to their excellent ability to absorb high amounts of energy when shot with high velocity projectiles [5,42]. Conventional body armors are composed of approximately 40 layers of woven fabric such as Kevlar [5]. Yarn rotation, lateral sliding, uncrimping, translation, plastic deformation and fracture mechanisms describe the ballistic and stab resistance of woven fabrics [43]. High performance woven fabrics are in general bulky and stiff. Hence, they can not provide soldiers with the required mobility, agility, and comfort when used as body armors. As well, the rigidity of these materials limits their use to only the torso protection. However, battlefield statistics indicate that 70% injuries located on extremities. This result brings on the requirement of flexible, lightweight, less bulky, and protective body armor design because of the particular risk of extremities. Besides, new protective vest should provide not only ballistic resistance but also puncture and cutting resistances. Lee et al. demonstrated that the impregnation of shear thickening fluid (STFs) improves the ballistic performance of Kevlar fabric because this composite structure can disperse the energy from a projectile or stab threat better than neat Kevlar [5]. The structural transition from fluid to solid like behavior in shear thickening fluid leads to considerable interest in the field of body armor. As a consequence, the liquid armor idea has accelerated the research on shear thickening fluids over the last few years. Houghton et al. have investigated the penetration resistance of shear thickening fluid impregnated fabric under a needle puncture [44]. The incentive behind this study was to protect people such as medical personnel who frequently come into contact with hypodermic needles. Needles can carry dangerous and infectious diseases. Thus, improvements of protective gloves are of vital importance because of particular risk to hands and fingers. As a conclusion of their work, they reported that the addition of STF improves the needle puncture resistance of fabrics due to decrease in yarn mobility.

Recent publications have also reported the usage of STFs for the body armor. One of them is composed of silica particles (450 nm average diameter) and ethylene glycol at volume fractions of $\varphi = 0.57$ and 0.62 [5]. Another one is a mixture of silica particles (450 nm average diameter) with a mass fraction of 67% (corresponding to an approximate volume fraction of 52%) and 200 molecular weight polyethylene glycol instead of ethylene glycol [49]. Also, some other researches have investigated the rheological behavior of different types of liquid media and particles to improve the penetration resistance under spike, stab, and ballistics threats. For instance, Rosen et al. have studied the rheology of 500 nm kaolin clay and glycerol [48]. Kaolin clay used in this work has nearly the same particle size as silica particles reported in above given works, but has platelet geometry unlike the spherical silica particles. This geometrical feature of clay particle provides higher spike and stab resistance for Kaolin-STF-Kevlar composite than Silica-STF-Kevlar one since plate like particles can be more efficient to disperse energy and distribute stress laterally. Also, the resistance to projectile was similar to the standart Si-STF-Kevlar composite. It is important to note that kaolin clay is commercially available and low cost materials so the clay based shear thickening fluids applications area can be widen without financial anxiety. Another STF formulation was reported by Kalman et al, which is composed of PMMA particles and the polyethylene glycol [45]. They stated that hard particles used in previous studies might damage the Kevlar filament and therefore softer particles PMMA was used in their work as a replacement for silica particles [49]. This formulation improved the spike resistance of the Kevlar fabric. However, it showed significantly less improvement under ballistic tests because the rheological behavior of this formulation exhibits a discontinuous rise in viscosity at critical shear rate in contrast to Silica-STF formulation. PMMA-STF showed second shear thinning regime at the highest shear rate. Also microscopy analysis of Kevlar-STF composite indicated that PMMA particles did not damage the filament, but particles were deformed after ballistic tests.

Referring to above given concise literature review, one can conclude that the addition of a shear thickening fluid in fabric armor leads to the design of a body armor with comparable ballistic properties to a neat Kevlar while being lighter and less bulky, and offering higher flexibility. Shear thickening behavior is a reversible process such that the rigidized colloid returns back to its initial fluid like nature upon the removal of the applied shear stress. All concentrated suspensions under right conditions can exhibit a shear

thickening behavior. However, in the literature, the exact conditions and the origin of shear thickening behavior are not well understood. In this direction, we have conducted detailed and systematic experiments to shed light on the origin and the mechanisms of shear thickening behavior of suspensions, which are flocculated initially albeit being stabilized by steric means, with the intention of being able to design an optimized liquid body armor system using STF/woven fabric. The suspensions studied in this work include low volume fraction, anisotropic, flocculated fumed silica particles with small fractal dimensions which correspond to a more porous structure. As a result of our experimental works, we have concluded that the two previously cited well known theories are not appropriate for explaining the shear thickening behavior of colloidal suspensions studied in this work since these two well known theories can explain the rheological behavior of suspensions being composed of monodisperse/ nonagglomerated hard sphere particles. In light of our experimental results, we suggest that the dominant effects for the occurrence of shear thickening phenomenon of studied suspensions are the increase in the total surface area of fractal particles due to the break up of compact flocs (hydrodynamic effect), and the raise in the effective volume fraction of particles. To be more specific, at low shear rates, there are compact flocs in our colloidal systems. The application of higher shear rates breaks down compact flocs into small aggregates and thus the total surface area of the dispersed phase increases. The increase in the surface area enhances the adsorption of liquid molecules on particles, and the fractal nature of fumed silica aggregates facilitates the fluid entrapment in porous structure. In what follows, the amount of non-adsorbed free liquid molecules in the system decreases, the mobility of polymer chains is also hindered by dispersed aggregate silica particles, and the lubrication effect among the aggregate particles deteriorates. Additionally, the decrease in the distance between fractal fumed silica aggregates due to the break-up of compact flocs increases the probability of interactions among themselves.

CHAPTER III

3. EXPERIMENTAL

3.1. Materials

The starting raw material was a commercial fumed silica powder, which was supplied by Wacker Chemie AG. Fumed silica is a synthetic, and amorphous form of silicon dioxide (SiO_2) produced via flame hydrolysis of silicon tetrachloride (SiCl_4) in a flame of H_2 and O_2 . The exposure of primary silica particles to high temperature during the production stage converts its structure into the form of aggregate which is unique properties of this type of silica particles. Therefore primary flow units in suspensions are aggregates, not individual particles of silica (see figure 3.1). In this work, two different types of fumed silica are used, namely hydrophilic (hfsi, N20) and hydrophobic (hpfsi, H15) fumed silica. BET surface areas of hydrophilic and hydrophobic fumed silica are 170-230 and 100-140 (m^2/g), respectively. In addition, the hydrophilic fumed silica silanol group (Si-OH) density is 2 SiOH/nm^2 whereas hydrophobic fumed silica silanol group density is 1 SiOH/nm^2 . Higher silanol density makes the surface of fumed silica hydrophilic (Si-OH); however, replacing silanol groups with another functional group ($-\text{OSi}(\text{CH}_3)_2-$) makes the surface of particles partially hydrophobic. In this study, the particle size and the distribution of fumed silica in various types of liquid media have been characterized by transmission electron microscopy (TEM) and dynamic light scattering (DLS).

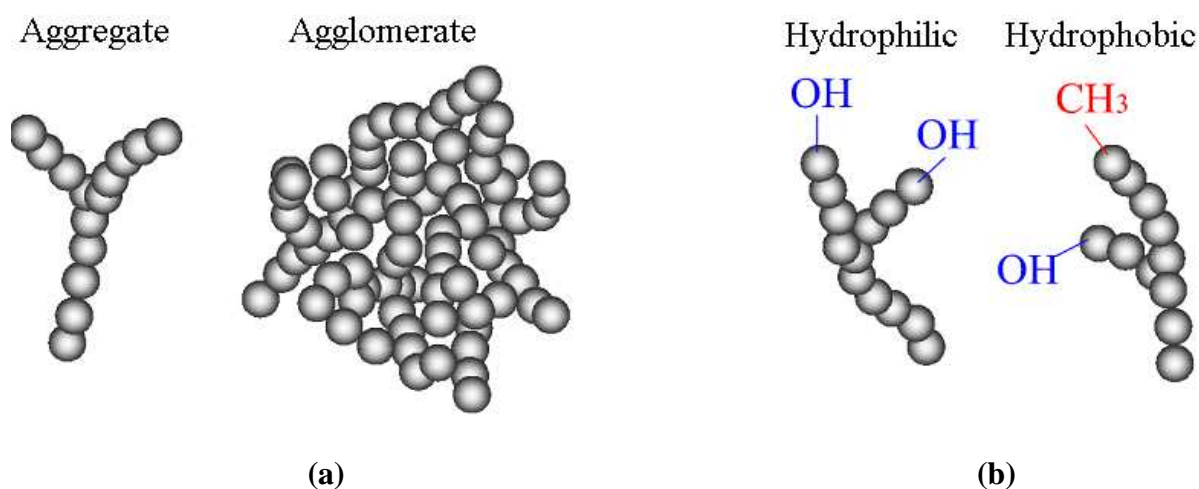


Figure 3.1. Schematic representations of (a) primary flow units (aggregate) and agglomerate structures of fumed silica, (b) the hydrophilic fumed silica (N20) which

contains hydroxyl functional groups on the surface and the hydrophobic fumed silica (H15) with both hydroxyl and methyl groups on the surface.

In this work, four different types of continuous phases (polyethylene glycol (i.e., $\overline{M}_n = 200, 300, 400, 600$ g/mole, Sigma-Aldrich), ethylene glycol (Sigma-Aldrich), glycerin (Sigma-Aldrich), and ethylene-propylene oxide copolymer (Dow Chemical)) were used to prepare colloids to be studied. Besides, Lithium Chloride (Fluka) were used to make conductive continuous media for the electrical resistance measurement experiments. Molecular structure and viscosity of these liquids are presented in table 3.1. The viscosity profiles of continuous phases were determined through a rotational rheometer (Malvern Instrument CVO Rotational Rheometer). These liquids have low viscosities and show Newtonian flow behaviors.

Table 3.1. Properties of continuous liquid phase used in this study.

Continuous phase	Molecular Structure	η at 25 °C (Pas)
Polyethylene glycol 200	$\text{HO-CH}_2\text{-(CH}_2\text{-O-CH}_2\text{)}_n\text{-CH}_2\text{-OH}$	0.056
Polyethylene glycol 300	$\text{HO-CH}_2\text{-(CH}_2\text{-O-CH}_2\text{)}_n\text{-CH}_2\text{-OH}$	0.077
Polyethylene glycol 400	$\text{HO-CH}_2\text{-(CH}_2\text{-O-CH}_2\text{)}_n\text{-CH}_2\text{-OH}$	0.102
Polyethylene glycol 600	$\text{HO-CH}_2\text{-(CH}_2\text{-O-CH}_2\text{)}_n\text{-CH}_2\text{-OH}$	0.140
Glycerin	$\begin{array}{c} \text{OH} - \text{C}_3\text{H}_5 - \text{OH} \\ \\ \text{OH} \end{array}$	1.500
Ethylene glycol	$\text{HO-CH}_2\text{CH}_2\text{-OH}$	0.017
Ethylene-propylene oxide copolymer	$\begin{array}{c} \text{CH}_3 \\ \\ \text{RO-}[\text{CH}_2\text{CHO}]_n[\text{CH}_2\text{CH}_2\text{O}]_m\text{-H} \end{array}$	0.161

3.2. Characterizations

The suspensions were prepared by adding particles into the associated liquids and mixing them for about 30 min at 5000 rpm. All silica concentrations were reported on a wt/wt

(silica/liquid) basis in Table 3.2. Rotational Rheometer (Malvern Instrument CVO Rotational Rheometer), Dynamic Light Scattering (*Malvern* Instruments Nanoseries Zetasizer instrument) and Transmission Electron Microscopy (FEI Company Tecnai, G2 Spirit BioTwin) studies were performed to study viscosity profiles under the steady shear and viscoelastic characterization under the dynamic shear, hydrodynamic radius (HR), and the microstructure of fumed silica in various types of liquid media, respectively. Rheological analyses were performed using a rotational rheometer (Malvern Bohlin CVO) in stress-controlled mode. All experiments were conducted at ambient temperature (25°C) by using a cone and plate geometry with a diameter of 40 mm and a cone angle of 0.02 rad. In all experiments, the distance between the tip of the cone and the flat plate is set to be about 70 μm for obtaining reproducible results. In order to remove the experimental artifacts, preshear (at a fixed rate of 1 s^{-1} for 60 s) was applied on each sample prior to any experiment.

Table 3.2. Formulations of studied suspensions.

	Particle Type	Continuous Media	Mw of Cont. Media (g/mole)	Particle Size	Mass/Volume Fraction of Particles	Preprocessing Speed
M1	HFSi	EG	62.07	30 nm	20 wt %, 11 vol %	5000 rpm
M2	HFSi	GLY	92.09	30nm	20 wt %, 11 vol %	5000 rpm
M3	HFSi	PEG	200	30nm	20 wt %, 11 vol %	5000 rpm
M4	HPFSi	EPO-PPO	1300	30nm	20 wt %, 11 vol %	5000 rpm
M5	HPFSi	PEG	200	30nm	20 wt %, 11 vol %	5000 rpm
M6	HFSi	EPO-PPO	1300	30nm	20 wt %, 11 vol %	5000 rpm
M7	HFSi	PEG	300	30nm	20 wt %, 11 vol %	5000 rpm
M8	HFSi	PEG	400	30nm	20 wt %, 11 vol %	5000 rpm
M9	HFSi	PEG	600	30nm	20 wt %, 11 vol %	5000 rpm
M10	HFSi	PEG	200	30nm	25 wt %, 13,75 vol %	5000 rpm
M11	HFSi	PEG	200	30nm	30 wt %, 16,5 vol %	5000 rpm
M12	HFSi	PEG	200	2 μm	20 wt %, 11 vol %	5000 rpm
M13	HFSi	PEG	400	30nm	20 wt %, 11 vol %	11000 rpm

Capacitance of the polyethylene glycol and ethylene oxide-propylene oxide copolymer within a parallel plate capacitor was measured by an LCR Meter (HIOKI 3532-50 LCR HiTester) in order to calculate the dielectric constants of these continuous media. For the capacitance measurement, we have used a home-made parallel plate capacitor that is composed of two parallel plates (made of a brass alloy) with a surface area S and plate-to-plate distance of d as shown in Figure 3.2. Figure 3.2 also shows the experimental configuration for measuring the electrical resistance of the colloid with a digital multimeter during the viscosity analysis. For the data acquisition, a LabVIEW (Laboratory Virtual Instruments for Engineering Workbench) program was written and used.

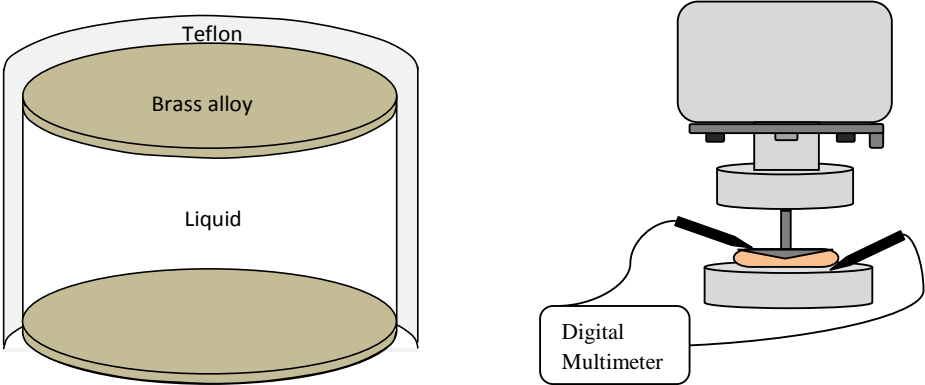


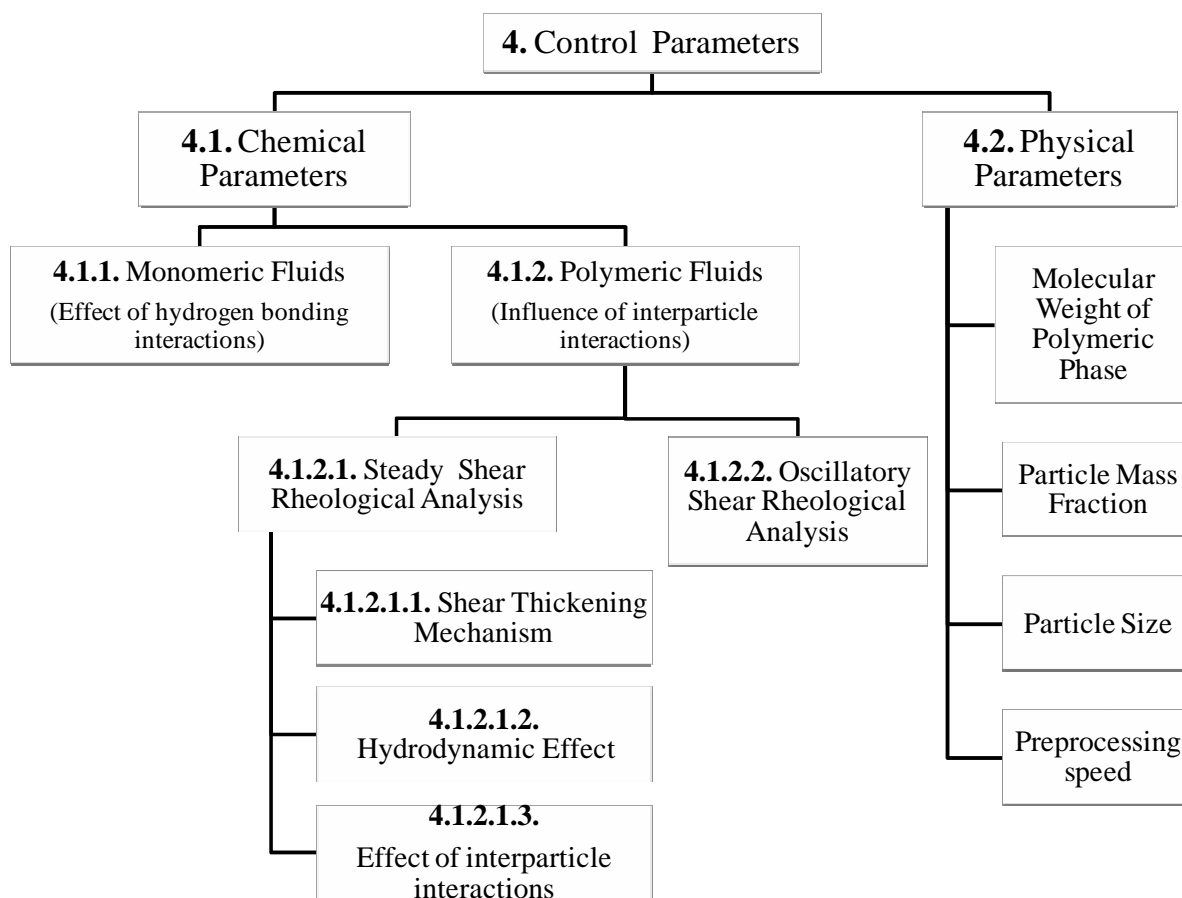
Figure 3.2. The schematic representation of a parallel plate capacitor (left), and the integration of the rheometer with the digital multimeter for the electrical resistance measurements (right).

CHAPTER IV

4. RESULT AND DISCUSSIONS

In light of our literature review, we are led to appreciate the necessity of a systematic and all-encompassing study which analyses the individual and combined effects of a wide variety of physicochemical and processing parameters (i.e., *suspended phase*: particle size, concentration, surface chemistry; *continuous phase*: monomeric or oligomeric continuous phases, molecular weight and preprocessing speed) on the shear thickening behavior of CNSs which are flocculated initially albeit being stabilized by steric means, in order to shed light on the mechanisms of this flow behavior.

Towards this end, we classify control parameters into two sub groups; namely, chemical parameters and physical parameters, which will be discussed in section 4.1 and 4.2, respectively (see schema 4.1). The paper is structured as follows: having described in section 4.1.1 influence of monomeric continuous phase and in section 4.1.2 effect of oligomeric continuous phase on the flow behavior of mixtures. In section 4.1.2.1, results of steady rheological experiments are discussed. Shear thickening mechanism of colloids which are low volume fraction, anisotropic and flocculated is explained with the result of electrical resistance and steady shear rheology experiment in section 4.1.2.1.1. We have also attempted to explain the studied rheological behavior of colloids referring to effects of hydrodynamics (in section 4.1.2.1.2) and interparticle interactions (in section 4.1.2.1.3). In hydrodynamic part, the effects of shear induced mechanical and hydrodynamical forces on the microstructure of the colloid and the associated changes in cluster sizes are discussed. In addition, the microstructure evolution is considered in view of interaction forces among particle-particle and particles-oligomer through thermodynamics considerations are described in effect of interparticle interaction part. In section 4.1.2.2, oscillatory shear experiments are also described to support our finding from section 4.1.2.1 about the microstructural and rheological change of system. Effect of physical parameters such as particle mass fraction, particle size, molecular weight of oligomeric phase and preprocessing speed on the rheological behavior of suspension are explained in section 4.2. The presentation is concluded with final remarks.



Schema 4.1. A schema that shows experimental parameters for studied nano colloids.

4.1. Chemical Parameters

In this part of the work, influence of surface chemistry of particles and hydrogen bonding ability of the continuous media with dispersed phase on shear thickening of CNSs, have been investigated. In this direction, the rheology of mixtures (M1-M6, see table 3.2) composed of hydrophilic/phobic fumed silica and four different liquid media (i.e., Ethylene glycol, glycerin, polyethylene glycol, ethylene-propylene oxide copolymer) have been studied. To have comparable results, in these experiments, the weight percent of constitutes in the mixture is fixed, namely, fumed silica (20 wt %). The findings of these experiments are summarized in Figure 4.1 and Figure 4.2 as a plot of viscosity versus shear rate. One of the six suspensions (M6) shows shear thinning behavior for a wide range of shear rates whereas remaining suspensions reveal shear thickening behavior. Furthermore, it should be noted that colloids M1, M2, M3, M4, and M5 appear to have measurable zero shear viscosities and do not show shear thinning from the very lowest shear rates. This is an obvious and expected

result noting that these colloids are composed of continuous phases exhibiting Newtonian flow behavior at this shear rate range and dispersed phases with low particle volume fractions.

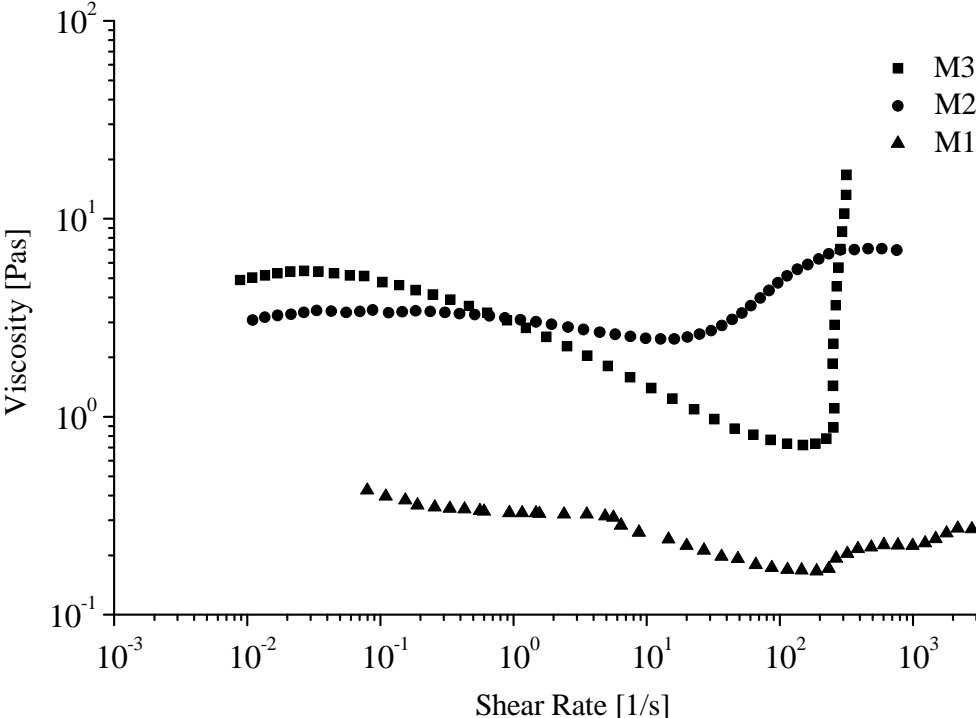


Figure 4.1. Steady rheological behavior of suspensions in order to understand the effect of hydrogen bonding capability of continuous media.

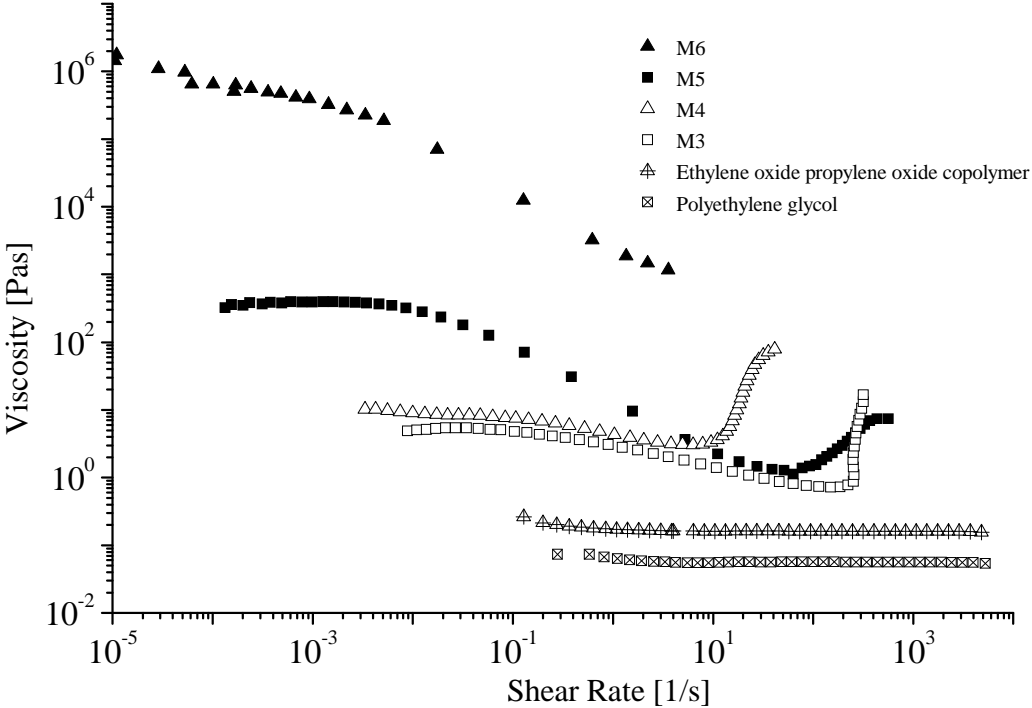
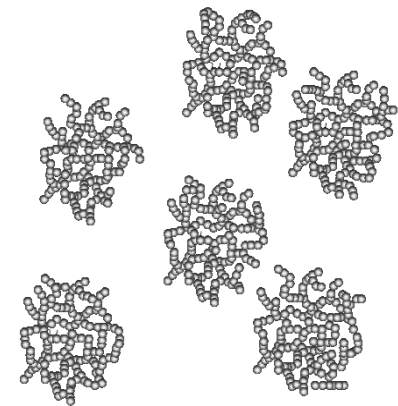
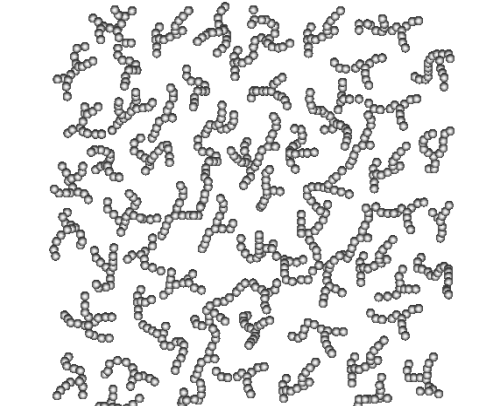


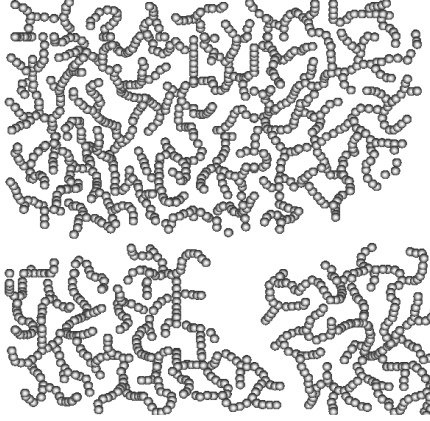
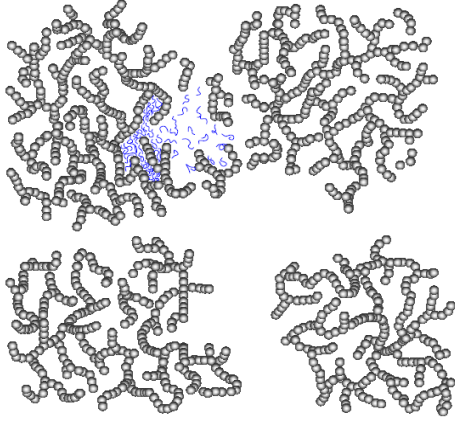
Figure 4.2. Viscosity versus shear rate profile of suspensions (M3-M6) and polyethylene glycol, ethylene propylene oxide copolymer

4.1.1. Monomeric fluids: Effect of hydrogen bonding interactions

As can be concluded from Figure 4.1, each colloidal suspension shows a distinct rheological behavior that can be attributed to the difference in the molecular structure of liquids and associated change of interfacial forces between constituents, which are elaborated in Table 4.1. The comparison of the viscosity profiles for the M1 (20 wt. % HFSi+EG) and M2 (20 wt. % HFSi+GLY) clearly reveals the influence of the interparticle hydrogen bonding on the shear thickening behavior. Therefore, it is prudent to continue with our discussion considering forces between particles in different continuous media. Note that the free energy G of two particles in an inert atmosphere decreases as the distance between their centers gets smaller since the surface energy is a function of both surface tension σ and the interfacial area A ; namely, $G = \sigma A$. On the other hand, the strength of the attractive force strongly depends on the nature of the particles and dispersion medium when particles are in the liquid medium [46].

Table 4.1. Schematic representations for microstructural changes of suspensions under shear.

	At lower shear rates	At higher shear rates
Shear Thickening Fluids	 <p>Low shear force can not destroy flocculated silica particles.</p>	 <p>Flocs are broken up and the viscosity increases due to the higher surface area of finely dispersed small aggregates.</p>

<p>Shear Thinning Fluids</p>	 <p>Bigger floc structures exist in shear thinning fluids due to the higher particle-particle interaction strength.</p>	 <p>Flocs structures are disrupted and relatively smaller size isolated agglomerates form when a shear is applied on the system. Therefore, trapped liquid molecules are released whereby the viscosity of the system decreases.</p>
-------------------------------------	--	--

The van der Waals attractive forces between particles can be calculated by using a relatively simple approximate equation given by Israelachvili [47] as

$$V = -A_{eff} (a/12H) \quad (1)$$

$$F = -dV / dH = A_{eff} (a/12H^2) \quad (2)$$

$$A_{eff} = \frac{3}{4} kT \frac{(\epsilon_c - \epsilon_d)^2}{(\epsilon_c + \epsilon_d)^2} + \frac{3h\nu_e}{16\sqrt{2}} \frac{(n_c^2 - n_d^2)^2}{(n_c^2 + n_d^2)^{3/2}} \quad (3)$$

where A_{eff} is the effective Hamaker constant, a is radius of sphere, H is a distance of closest approach between two identical sphere, V is the pair potential, ϵ is the dielectric constant, n is the refractive index, h is the Planck's constant, k is the Boltzmann constant, T is the absolute temperature and the parameter ν_e refers to the main electronic absorption frequency for the dielectric permittivity ($3 \times 10^{15} \text{ s}^{-1}$ assumed to be the same for both media [52]). Here, subscripts c and d in the above relation denote the continuous medium and the dispersed phase, respectively. It should be noted that the above formulations hold correct for

spherical particle geometry. Nevertheless, we have used these formulations to calculate vdW interactions between the particles in our colloids with an anisotropic aggregate neglecting the particle geometry related errors in our calculations since our interest is on the comparison of the attractive vdW interactions between particles in different continuous medium. It can be deduced from the effective Hamaker constant relation that the closer the values of ϵ_c and ϵ_d to each other, the smaller the value of A_{eff} is. Hence, the attractive forces between particles decrease. The above force formulation suggests that colloidal particles attract each other always unless the dielectric constants and refractive index of particle and dispersion medium are the same. Effective Hamaker constant of particles in ethylene glycol and glycerin environments were calculated through using dielectric constants and refractive index of constituents (see table 4.2) in order to understand flocculation tendencies of particles due to the van der Waals attractive force.

Table 4.2. Dielectric constant and refractive index of constituents of suspensions (M1, M2, M3)

	Dielectric Constant	Refractive Index
Hydrophilic Fumed Silica	3.75	1.462
Hydrophobic Fumed Silica	2.60	1.460
Ethylene Glycol	37	1,431
Glycerin	47-68	1,473
Polyethylene glycol 200	16.13	1.459

Results indicate that effective Hamaker constant and vdW attraction of particles in M1 ($2.286 \times 10^{-21} \text{ J}$) is very close to particles in M2 (changes from $2.26 \times 10^{-21} \text{ J}$ to $2.5 \times 10^{-21} \text{ J}$). As a consequence, we have to investigate origin of the repulsive forces that give rise to different hydrodynamic radius of same particles in ethylene glycol and glycerin environments. Ethylene glycol has two hydroxyl groups, whereas glycerin has three hydroxyl groups, thereby possessing higher hydrogen bonding affinity towards silica particles. As a result of this, oligomer-particle interaction of suspension M1 is smaller than M2 due to existence of smaller number of hydroxyl groups in the molecular structure of the continuous matrix hence

the flocculation tendency of particles is higher in M1 since vdW attraction of particles are similar. It is known that in strongly hydrogen-bonding liquids, the interaction between the liquid molecules and surface silanol groups (Si-OH) of silica particles causes the formation of a solvation layer on the silica surface, which creates short-range non-DLVO repulsions [44]. Such repulsive forces due to the interactions between the surface hydroxyl of silica and liquid molecules precludes the aggregation of the silica particles, hence giving rise to a mixture with particles of smaller Hydrodynamic Radius (HR), and larger surface area. In what follows, one should expect that the HR of silica particles in glycerin is to be smaller than that in ethylene glycol. This argument is supported with the results of Dynamic Light Scattering (DLS) measurements used to determine the HR of silica particle in glycerin environment (147 nm) and in ethylene glycol environment (193 nm). As stated previously, in M2, the strength of particle-liquid interaction is greater than the particle-particle interaction in comparison to the M1 system; consequently, silica particles have smaller aggregates and larger effective surface area in glycerin. This is why zero shear viscosity of M2 is noticeably higher than M1 as presented in figure 4.1. As the shear rate increases, the ethylene glycol system exhibits slight increase in viscosity, whereas the suspension of silica and glycerin shows shear thickening after reaching a critical shear rate, see figure 4.1. This difference is due to the fact that, the glycerin system requires less shear force to break up (fragment) already smaller agglomerates, and in turn experience shear thickening at lower critical shear rate due to the further increase in the surface area.

The suspension M3 (20 wt. % HFSi + PEG) shows a sharp transition from shear thinning to shear thickening state while the colloid M1 (20 wt. % HFSi+EG) acts like a Newtonian fluid. In addition DLS measurements showed that the HR of colloids in M3 (164 nm) is smaller than that in M1 (193 nm) although both continuous media have two hydroxyl end groups. This difference can be explained by van der Waals attraction between particles in different continuous media and steric stabilization controlled by the adsorbed layer thickness of polymer on particles. Effective Hamaker constant of particles in M3 (1.960×10^{-21}) is smaller than M1 (2.286×10^{-21} J). Therefore, under these conditions the dispersion M1 might have higher tendency to flocculate than M3. Having dwelled on the strength of vdW attraction forces, one should also consider the dispersion forces since the adsorption of polymer on particle surfaces reduce attractive forces at all separations. The magnitude of the repulsive forces arising from the presence of adsorbed layer is linearly proportional to the density and

molecular weight of the dispersion media on the surface. The density of adsorbed layer on the particle surface in M1 and M3 might be similar since ethylene glycol and polyethylene glycol have same affinity towards to particle surface since both of them have two hydroxyl end groups. On the other hand, the adsorbed layer thickness is thinner in mixture M1 since the molecular weight of ethylene glycol is smaller than polyethylene glycol. The cumulative effect of stronger vdW attraction force and weaker steric force due to adsorbed layer thickness causes the formation of bigger flocculated structure in suspension M1. The zero shear viscosity of M3 is greater than that of M1 as can be seen in figure 4.1. This might be attributed to greater particle spacing within flocs in M3 considering their adsorbed layer thickness. In M3, the free ends of oligomer molecules adsorbed on particles extend into the oligomeric continuous phase and interact with available oligomer molecules and cause entrapment of these molecules within flocculated structure formed due to the existence of vdW attraction force. On the other hand, in M1, the adsorbed layer thickness is smaller in comparison to M3 since the continuous phase is a monomer. Therefore, particles in M1 can form more compact flocs that do not contain entrapped fluid molecules.

4.1.2. Polymeric fluids: Influence of interparticle interactions

To address the influence of the colloidal interactions on the extent of shear thickening, the rheological and microstructural traits of suspensions composed of fumed silica with dissimilar surface chemistry and different polymeric media (table 3.2 & figure 4.2) have also been studied. Rheological characterization was carried out using several *simple* controlled methods, steady shear, oscillatory shear and the results of these tests are quantified using material functions such as steady viscosity, storage and loss modulus, respectively. Considering the interaction abilities of constituent phases, colloidal suspensions can be classified as Lyophilic and Lyophobic. In Lyophilic colloids, the dispersion media molecules have higher affinities towards the surface molecules of dispersed phase. In the following, we present the rheological and the micro structural traits of four Lyophilic colloids (i.e., M3, M4, M5, M6) with different degrees of polymer-particle interaction strength to clarify the effect of the colloidal interactions on the extent of shear thickening. Recalling that when there is a strong interaction between silica particles and polymer molecules, solvation layers form on silica surfaces, thus giving rise to short range repulsive forces. The higher the repulsive forces are, the smaller is the flocculation tendency of initial aggregates (as received samples) and

hence, less shear force is required to break down already small size flocs and subsequently transform them into aggregates. Therefore, for the polymeric/oligomeric colloids to show shear thickening behavior, the polymer/oligomer-particle interaction strength should be higher than the particle-particle interaction strength.

4.1.2.1. Steady shear rheological analysis

In the following, we have discussed the experimentally observed non-Newtonian flow behavior in suspensions of M3, M4, M5, and M6 in light of above provided discussions through referring to both effects of shear induced mechanical and hydrodynamical forces (in section 4.1.2.1.2) and interparticle interaction (in section 4.1.2.1.3). Given that the suspension M3 (table 3.2) shows shear thickening under steady shear (figure 4.2), one can expect preferential interactions between hydroxyl end groups of the continuous media and surface hydroxyls of silica particles (figure 4.3.a). As stated earlier, referring to Eq.3, colloidal particles always attract one another unless dielectric constant and refractive index of particle and dispersion medium are the same [52]. In addition, existence of solvation layer on the particle surface due to polymer-particle hydrogen bonding interaction create steric repulsive force [44]. For steric stabilization to be effective polymer should be attached to the surface by strong adsorption to create dense adsorbed layer and sufficient chain length should enable an adequately large value of adsorbed layer. Therefore, in lyophilic colloids with low molecular weight of adsorbed oligomer, the oligomer-particle interaction through the hydroxyl creates weak steric forces. These weak repulsive forces are unable to prevent attractive particle-particle interaction. However, they may change the strength of van der Waals attractive force. In M3, the magnitude of the steric repulsive forces arising from the presence of adsorbed layer is small since low molecular weight of polyethylene glycol (200 g/mol) cannot provide an adequate steric barrier. Consequently, particle-particle attractive interactions in the system still exist, but weakened by steric effect. That is why small flocculated structures form in the colloidal system. The three orders of magnitude difference between the zero shear viscosity of PEG and the M3suspension (0.0055 Pas, 5 Pas respectively in figure 4.2) imply the existence of flocculation in M3 because highly flocculated colloids are known to possess high viscosity values at low shear rates. The fact that measured hydrodynamic radius (HR) of particles (164 nm) in M3 is significantly larger than the aggregate size of as-received particles (~30 nm) further supports floc formation even though performing DLS on these suspensions require

considerable dilution which can destroy some agglomerate or floc structure in suspensions. It is a crucial to note that in contrast to previously stated two well known theories, the steady rheological data of M3 show shear thickening behavior over a narrow range of higher shear rates despite the fact that flocculated and anisotropic structures exist in the system.

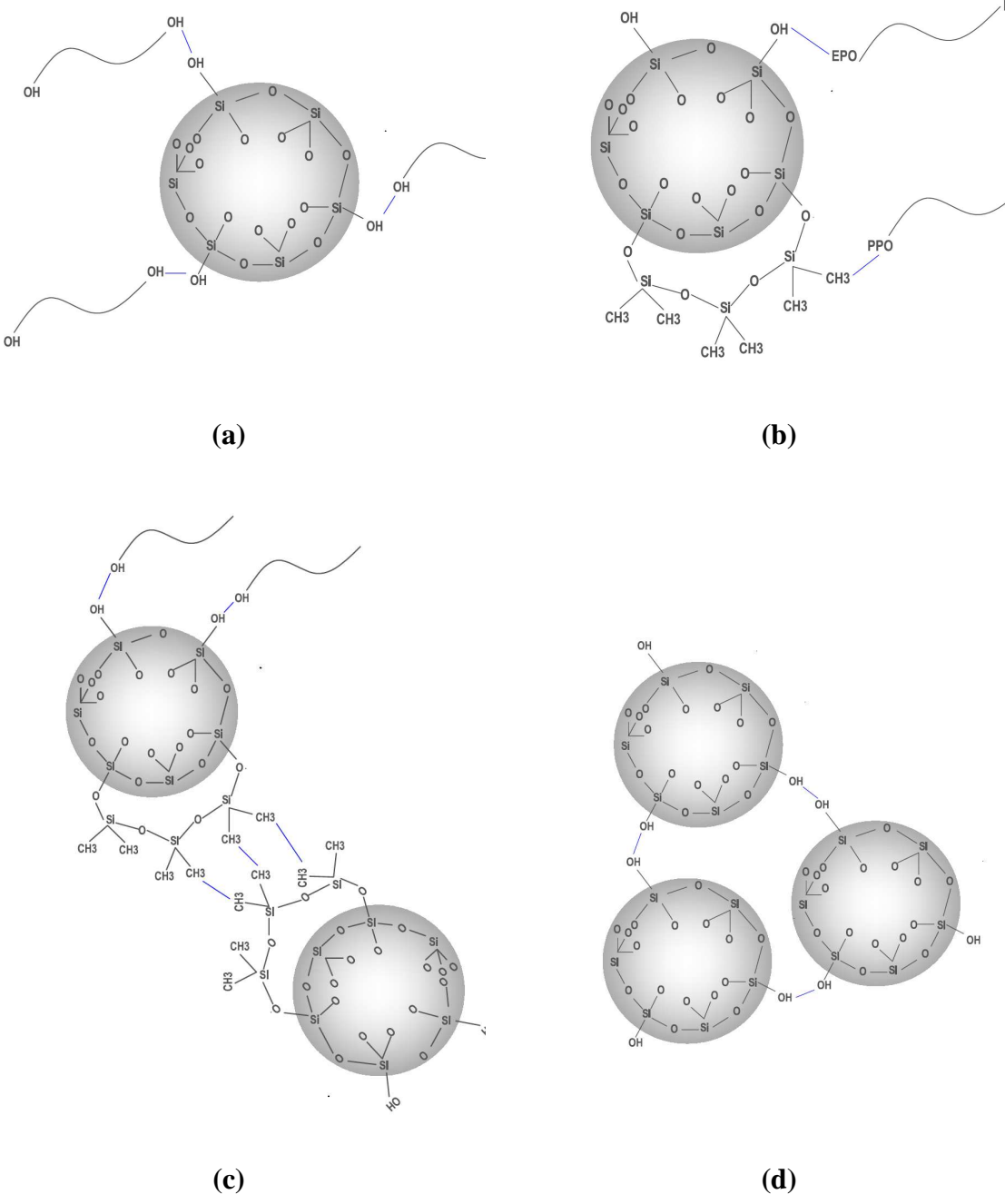


Figure 4.3. Schematic representations for interparticle interactions in dispersions of (a)

M3, (b) M4, (c) M5, (d) M6.

4.1.2.1.1. *Shear thickening mechanism*

To be able to comment on the relation between colloids' microstructure and rheology, we have measured the electrical resistance of a shear thickening suspension (M3) composed of polyethylene glycol and hydrophilic fumed silica under a shear or without a shear. In electrical resistance experiment, we used suspension M3 because it shows shear thickening behavior. To make this suspension a mixture of insulating particles and conductive continuous media, lithium chloride (1 wt%) was dissolved in polyethylene glycol. In an experiment, the electrical resistance of the dispersion was monitored as a function of time in the absence of shear force as shown in figure 4.4. Figure 4.4 indicates that the electrical resistance decreases rapidly during the first 20 seconds and then levels off. In an another experiment, the electrical resistance of the suspension M3 was also measured under the applied shear force during the viscosity measurement with the purpose of examining microstructural change due to the application of increasing shear force. Figure 4.4 demonstrates that in the first 20 seconds, the electrical resistance of the suspension M3 recorded under a shear force shows somewhat similar behavior with that measured in the absence of a shear force. During the latter experiment, we have also recorded viscosity versus shear rate and time data as plotted in figure 4.5 whereby it is observed that the viscosity decreases between 20 and 50 second while the electrical resistance is nearly constant at this time interval. At low shear rates, silica particles are in the form of densified flocs. The free/unadsorbed oligomer chains act like a lubricant between these flocs in shear thinning regime since they are aligned along the flow direction, thereby leading to an increase in the flowability while a decrease in the viscosity of the suspension. Moreover the conducting continuous media flows easily between adjacent silica flocs so the electrical resistance of the suspension does not change. After this time interval the viscosity starts increasing monotonically whereas the electrical resistance experiences a sharp jump over a short processing time span and subsequently levels off. In view of figures 4.5, and the pertinent previous explanations, one can conclude that the microstructure of the colloid changes due to the applied shear force. As mentioned earlier, at low shear rates, the compact flocs exist in colloidal systems. The application of higher shear rates breaks down compact flocs into small aggregates and thus the total surface area of the dispersed phase increases (figure 4.5). Due to

the increase in the surface area of the non conductive dispersed media, the distance between the fractal fumed silica aggregates decreases, which brings about the higher interaction tendency among particles under the shear whereby the viscosity increases. As for the increase in the electrical resistance of the colloid, it is related to the fact that the conductive oligomer chain cannot penetrate easily into gaps between non-conductive fumed silica aggregates. The following argument might also have an effect on the increase of the viscosity. Just as an analogy if finely dispersed aggregates were considered to be an array of obstacles in a flow field, then they would hinder the motion of the oligomeric phase. Therefore, the viscosity is expected to increase in colloids with large particle surface area (finely dispersed particles) due to the reduced mobility of oligomer chains.

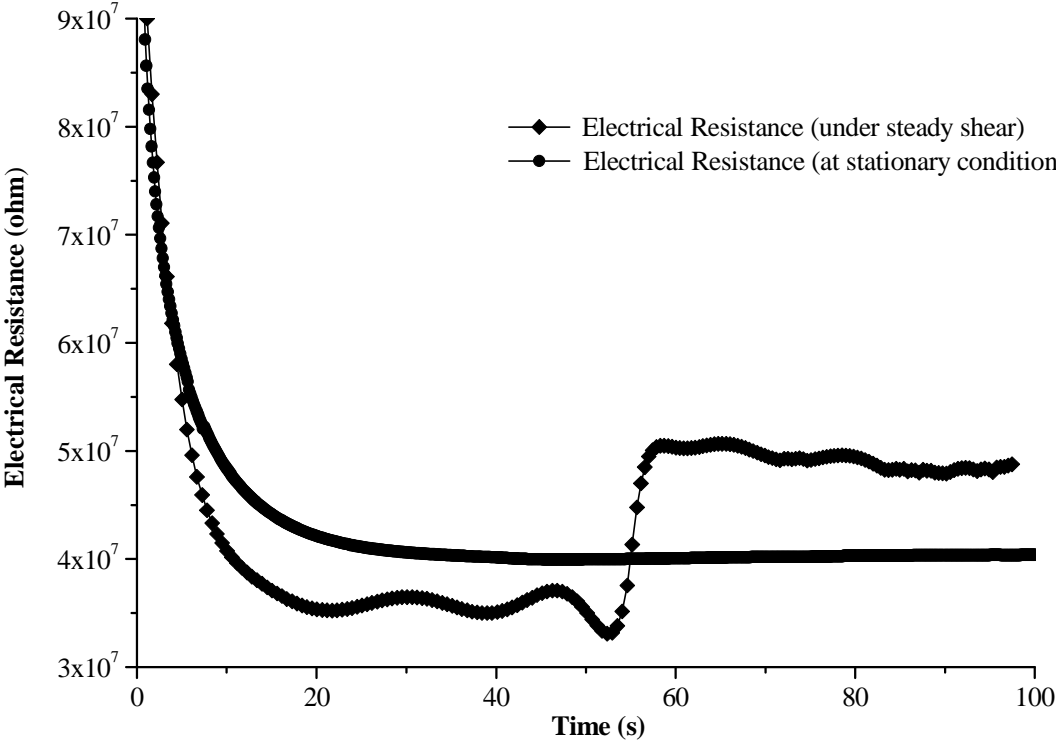


Figure 4.4. The electrical resistance measurements of HFSi+Peg+Lithium chloride dispersion under the applied shear during the viscosity analysis, and without the applied shear at the stationary condition.

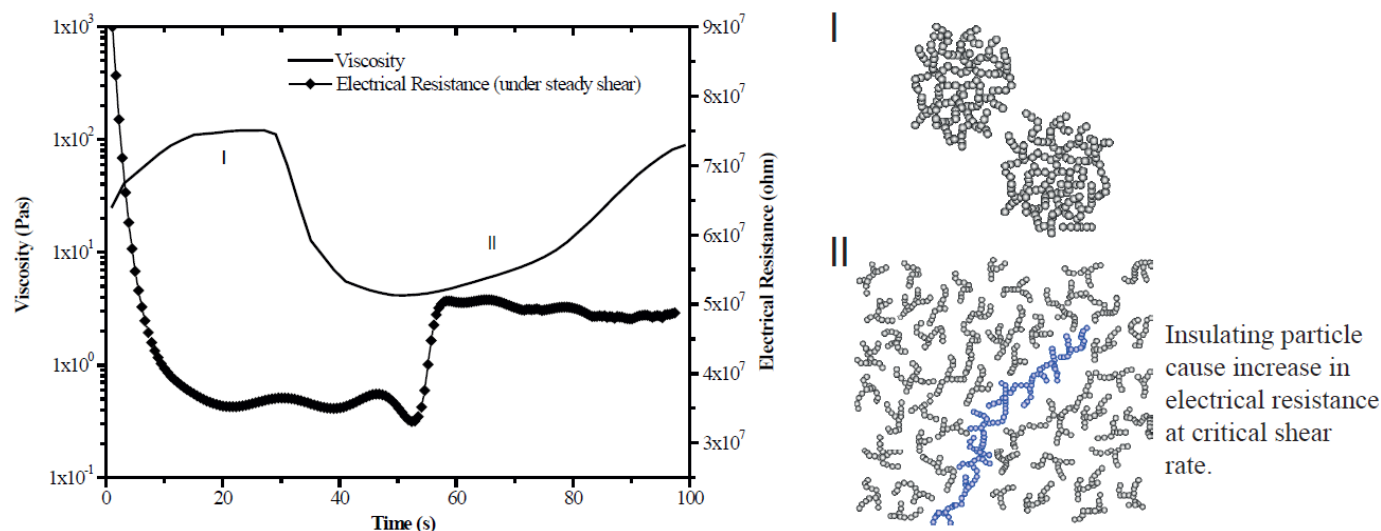


Figure 4.5. Viscosity and electrical resistance versus time plot of the HFSi+Peg+Lithium chloride mixture and a schematic representation for the microstructural change in a mixture under the shear.

4.1.2.1.2. *Hydrodynamic effect*

In this section, we will briefly discuss several possible hydrodynamic mechanisms which may contribute to the occurrence of shear thickening in CNS studied in this work. Figure 4.6.a exemplifies the flow in a concentrated and monodisperse dispersion. In such a system, the flow takes place due to the particles rolling past one another given that particles are nearly close packed ($\phi=0.625$; volume fraction, for close packing of spheres) at rest and the liquid continuous media is sufficient to fill void spaces. If there were no adequate amount of liquid to fill the additional void spaces generated by the application of high shear (figure 4.6.b), the direct solid-solid contact would be encouraged and in turn the shear stress would increase, thereby leading to a rise in the viscosity with increasing shear rate [48,51]. It is thought that the above described shear thickening mechanism is also active to some extent in our shear thickening colloids. In the present shear thickening colloids (especially M3 and M4), the dispersed media is in the form of small compact flocs which can entrap a small amount of polymeric/oligomeric liquid within themselves (figure 4.7.a), and the big portion of the continuous phase in the colloid stays as unentrapped and/or unadsorbed polymer/oligomer chains. These free polymer/oligomer chains acts as a lubricant for the motion of each flocs past one another since they are aligned along the flow direction at low shear rates. The

application of higher shear force breaks down compact flocs into small aggregates thereby increasing the total surface area of the dispersed phase. The increase in the surface area of particles brings about the formation of large voids in between the branched structures of porous aggregates as illustrated in figure 4.7.b. Additionally, the fumed silica aggregates have small fractal dimensions [13]. The fractal dimension describes the size dependence of the particle mass and the small fractal dimension corresponds to more porous structure. Therefore, fractal aggregates can be considered to have ‘holes’. In view of these points, two main reasons can be suggested for explaining the increase of viscosity after the critical shear rate; first, the amount of continuous phase is insufficient to fill the additional void space generated by the breakdown of flocs into small aggregates due to the high shear applied, and second, the continuous phase is consumed to occupy holes on the surface of fractal silica aggregates. As a result, the continuous phase cannot behave as an effective lubricant between solid phases, hence leading to the augmented direct contact and friction between particles and in turn the increase in the viscosity of the colloid.

Additionally, considering the amount of fluid between flocs (present at low shear rates) and between aggregate structure (present at high shear rate) may also provide an alternative explanation for shear thickening. One may conclude from figures 4.7.a and 4.7.b that the thickness or the amount of fluid between aggregates is much less than that between flocs since the surface area of the dispersed phase has increased at high shears rates. The decrease in the fluid thickness between adjacent aggregates leads to an increase in the velocity gradients and the associated shear stress between two neighbor aggregates. Consequently, as the shear stress increases, so will the viscosity of the fluid since there is a linear dependence between them.

We previously noted that in our colloids, the aggregates are of anisotropic structures, and are aligned at different orientations with respect to flow fields as sketched in figure 4.8. Assuming that the shear applied on a colloid leads to a velocity profile given in figure 4.8, the upper and lower section of particles will experience different velocity fields. When a particle is at 90° to the direction of the shear field, its top and bottom will move at velocities $V + h(dV/dZ)$ and $V - h(dV/dZ)$ where V is the center velocity of the particle where variables are defined in figure 4.8. The rotational motions of anisotropic particles are strongly dependent on the turning moment and hence the angular velocity. The turning moment

changes with the orientation of anisotropic particle relative to the direction of the shear field. Hence, both moment and angular velocity is greatest when the particle is at 90° position. On the other hand, the rotational motion of the particle which is parallel to the shear field is slower than the particle that is 90° since h is bigger than h' . Consequently, motions of fast particles are restricted by slower particles and flowability of constituents decreases. This situation may also contribute to the increase in the viscosity of the colloid.

To further elaborate on the rheological attributes of M3 suspension, it is prudent to consider the adsorption of *polymers* at the surface of *dispersed particles* since this suspension is of a lyophilic character. When dispersed particles are covered by adsorbed polymer layers, their effective radius and the effective volume fractions become greater than that of the core particles since adsorbed polymer layers prevent particles from approaching to each other. As stated previously, higher shear rates break down compact flocs into small aggregates. Therefore, both the surface area and effective volume of particles increase whereby polymer chains can find more available sites on particle surfaces for adsorption. It should be noted that the adsorbed polymer chains hinder the motion of free polymer chains. The effective volume fraction and the intrinsic viscosity are related to the adsorbed layer thickness through equations $\phi' = \phi(1 + \delta/a)^3$ and $\eta = 2.5(1 + \delta/a)^3$, respectively where a is the particle radius, δ is the thickness of the adsorbed polymer layer, ϕ is the volume fraction of a particle and ϕ' is the effective volume fraction [49]. Noting the linear dependence between the viscosity and the effective volume fraction ($\eta = 2.5\phi'/\phi$), the increase in effective volume fraction at high shear rate increases the viscosity of the system [54]. Essentially, the increase in total surface area and effective volume fraction of particles reduces mobility of polymeric chains due to the combination of above effects hence leading to an increase in the viscosity of the system.

At low shear rates, the structure of the dispersed phase is controlled by the balance of the Brownian and interparticle forces, while at high shear rates it is governed by hydrodynamic forces. Therefore, it is sensible to consider the effect of the flow field on the microstructure of colloids. The hydrodynamic effects may cause a stable dispersion to aggregate under certain conditions by which the hydrodynamic clustering theory was explained in literature. When a suspension is subjected to a simple shear, a colliding pair of particles is compressed along the compression axis of the shear field and consequently form particle clusters oriented at 45°

with respect to the flow direction if the drag force on particles are strong enough. Stokes drag force acting on a collision doublet in a simple shear is written as $f_d = 6\pi\eta_o a^2 (dV/dZ) 2 \sin 45 \cos 45$. Here, η_o is the viscosity of medium, a is the particle radius and dV/dZ is the velocity gradient. One can note that the Stokes drag force $f_d = 6\pi\eta_o a^2 (dV/dZ)$ increases with the square of the particle radius [54]. Thus, particles with μm level radius are expected to be much more sensitive to the shear-induced aggregation than those with nanometer level radius [54]. In light of this fact, one can conclude that the hydrodynamic clustering theory can not accurately explain the shear thickening behavior of suspensions studied in this paper since the sizes of the dispersed phase in these colloids are nanometer size in shear thickening regime.

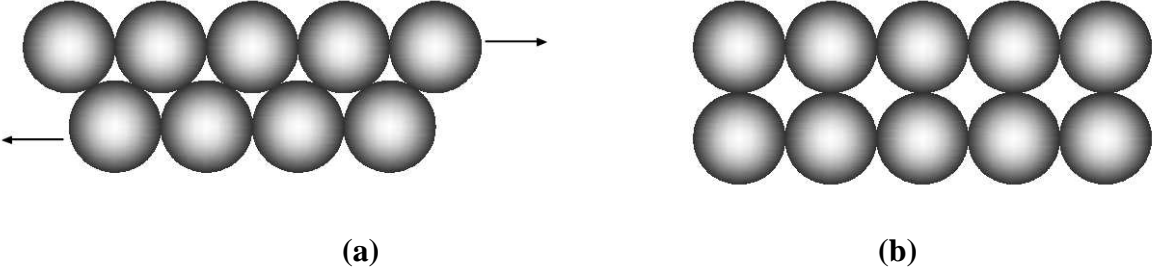


Figure 4.6. A schematic representation for shear thickening in a concentrated, spherical, monodisperse and close packed colloid system, (a) the relative motion of particles at low shear forces, (b) the increase of the viscosity due to the formation of extra void volume at high shear forces.

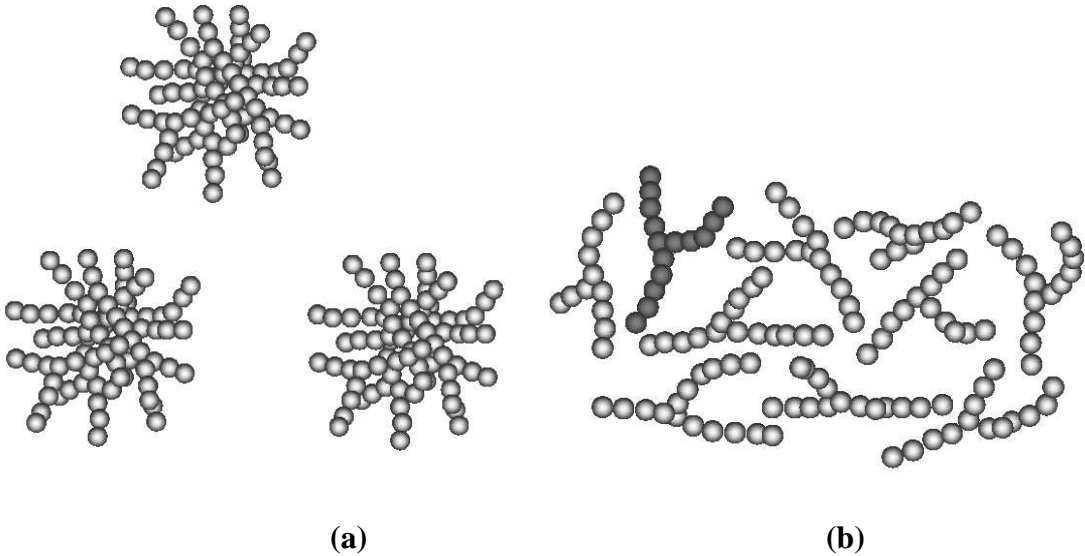


Figure 4.7. A schematic representation for the shear thickening in a concentrated,

anisotropic, polydisperse colloid system, **(a)** the relative motion of small flocculated particles at low shear forces, **(b)** the increase of viscosity due to the increase of particle surface area and formation of extra void volume between them at high shear forces.

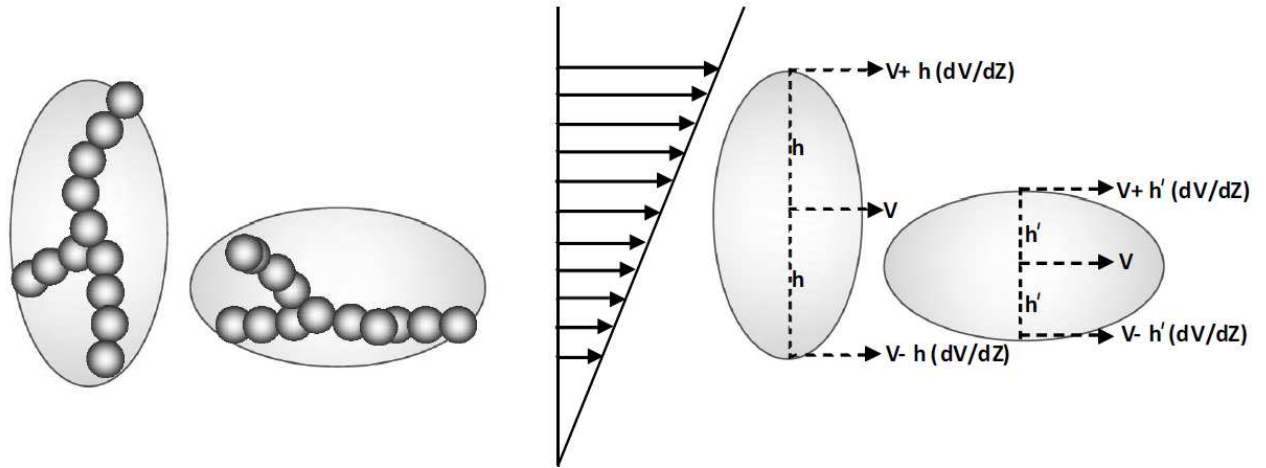


Figure 4.8. Rotational motion of an anisotropic particle induced by a shear field.

4.1.2.1.3. Effect of interparticle interactions

Here, we discuss the effect of interparticle forces on the rheological behavior of colloids since the interparticle forces also significantly affect the microstructure and in turn the rheology of nanocolloids. To do so, two important questions need to be asked; namely, under what conditions will dispersions flocculate or remain in a dispersed state? Since answers to these questions are closely related to the interparticle forces, it is vital to discuss the origin of these forces with thermodynamics considerations. Considering a colloid as a thermodynamics system with a constant temperature and pressure, the logical state function for the colloid will be the Gibbs free energy, G . The free energy of two particles in a colloid increase when the distance between their centers gets bigger due to the fact that the surface energy is a function of both surface tension, σ and the interfacial area, A ; namely $G = \sigma A$. These two colloidal particles attract one another and form an aggregate in order to decrease the total surface area and the free energy of the system. The stability of colloids is closely related to the shape of total free-energy curve which depends on the relative strength of attractive and repulsive forces. Colloidal dispersions with high free energy tend to move to a lower free energy state spontaneously when the energy barrier between the thermodynamics states is reduced or eliminated by adjusting the repulsive and attractive forces. In general, instability and flocculation are caused by a small free energy barrier. The colloid might be trapped at high

energy state with a sufficiently high energy barrier. In this case, the colloid is said to be meta-stable. However, the transition from this meta-stable state to a lower energy state will occur over a very long time span, effectively, the system can be considered at stable or the minimum energy state. The stability of colloidal system is controlled by the factors that determine the height of the energy barrier such as *chemical properties of the medium, surface and physico-chemical properties of dispersed phase, temperature and pressure* [51].

When particles are in a liquid medium, the strength of the attractive force strongly depends on the nature of the particles and dispersion medium, which can be calculated using the relation given by Israelachvili et al. (see equation 1, 2 and 3) [52]. It can be deduced from the effective Hamaker constant relation that the closer the values of ϵ_c and ϵ_d to each other, the smaller the value of A_{eff} is. Hence, the attractive forces between particles decrease. The force formulation given in equation 3 suggests that colloidal particles attract each other always unless the dielectric constants and refractive index of particle and dispersion medium are the same. It should be noted that the formulations hold correct for spherical particle geometry. Nevertheless, we have used these formulations to calculate vdW interactions between the particles in our colloids with an anisotropic aggregate neglecting the particle geometry related errors in our calculations since our interest is on the comparison of the attractive vdW interactions between particles in different continuous medium. In order to determine the dielectric constant of constituents for the calculation of Hamaker constants, we have measured capacitance of the polyethylene glycol and ethylene oxide-propylene oxide copolymer within the parallel plate capacitor by using LCR Meter. Using the measured capacitance, the dielectric constant were calculated through the relation $C = \epsilon_c \epsilon_o S / d$ where C is the capacitance of the fluid, ϵ_c is the dielectric constant of polymer, ϵ_o is the dielectric constant of the free space ($\epsilon_0 \approx 8.854 \times 10^{-12}$ F m⁻¹), S is the area of the lower and the upper plates, and d is the separation distance between the plates. Dielectric constant of particles and continuous media and the effective Hamaker constant are given in table 4.3 in order to compare van der Waals force of attraction between particles within different dispersion media.

Having addressed how particles attract each other, we should also consider repulsive forces (dispersion forces that give rise to the colloidal stability) especially when the space

between particle surfaces is filled with liquid. As the existence of liquid between particles reduces attractive forces at all separations and repulsive forces become effective, the free energy curve is modified. Colloid particles may repel one another by the electrostatic repulsive force. Many interfaces in aqueous systems carry electrical charges and like charges repel each other. Electrostatic stabilization in non-aqueous media is not as effective as in aqueous systems. Morrison et. al and Raghavan et. al demonstrated that the electrostatic stabilization is strongly dependent on the particle concentration in non-aqueous media and indicated that the electrostatic stabilization is not possible in non-aqueous systems at *high particle concentrations* [44,50]. Since the particle concentration of our systems is 20 wt%, the electrostatic forces play negligible stabilization role in comparison to the steric stabilization. In view of the fact that all of our suspensions possess a lyophilic character, the steric stabilization effect should be significant in these colloids due to the interaction between polymers and particles. In steric stabilization, the adsorbed layer may affect the interparticle forces in two ways; that is, it may change the strength of van der Waals attractive force and gives rise to a repulsive force between particles. For the steric stabilization to be effective, long enough polymer chains should be firmly attached to particle surfaces thereby forming a compact layer there. Furthermore, in the case of a suspension that is composed of particle, polymer and solvent, adsorbed polymer chains extend into the solvent due to the similar chemistry of the polymer and solvent. Consequently, surfaces cannot approach each other too closely because of the extension of adsorbed chains. Figure 4.9.a shows two particles with adsorbed polymer layer where a the radius of the particle and δ is the thickness of the adsorbed layer. The magnitude of the repulsive forces arising from the presence of adsorbed layer strongly depends on the density and molecular weight of the polymer on the surface. When the adsorbed polymer layer is dense enough, the center of the particles is precluded to come closer than $2(a+\delta)$. Brownian motion causes collisions between particles and the outermost parts of the layers start to mix as the molecules interpenetrate. The interpenetration of adsorbed chains increases the local density of polymer segments. Osmotic effect drives surfaces apart in order to reduce the segment concentration. This situation can also be explained by a thermodynamic consideration. The increased concentration of chains between surfaces restricts the motion of them, thereby leading fewer possible configurations available to each molecule. Consequently, the reduction in entropy (ΔS) causes an increase in the free energy. Entropic repulsion increases the center to center separation of particles. On the other

hand, if polymer density in the layer is lower, then attraction will be unaffected by the presence of the surface layer (figure 4.9.b). Moreover, short polymer chains on the surface cannot provide an adequate steric barrier. Finally, it is clear that density of the attached polymer chains on surface should be sufficient and the chain length should enable an adequately large value of δ in order to take the advantage of the steric stabilization. The small value of the adsorption thickness ζ ($<\delta$) and the polymer density of the layer are unable to prevent the particles from approaching one another. To this end, not only the existence of polymer but also the molecular weight and concentration create different effects on the system. As an example, the presence of an excess non-adsorbed polymer leads to decrease in flocculation while the existence of high molecular weight adsorbed polymer which are at low concentration causes flocculation of particles by bridging mechanisms.

To recapitulate, the total free energy of interactions between two colloidal particles can be written as sum of energies associated with van der Waals, electrostatic, steric, and other effects respectively as $\Delta G = \Delta G_{vdW}^a + \Delta G_{es}^a + \Delta G_s^r + \Delta G_o$ where the superscript a and r denotes the attractive and repulsive natures of the above free energies, respectively [51]. The cumulative effect of interactions between the liquid and solid particles may change the interparticle interaction, the microstructure and in turn the rheological behavior of the suspension.

Table 4.3. Dielectric constant, refractive index of constituent and the effective Hamaker constant of mixtures. Note that dielectric constants of our particles are compiled from literature.

	Dielectric constant	Refractive Index	Effective Hamaker constant (J)	
Hydrophilic Fumed Silica	3.75	1.462	M3	1.960×10^{-21}
Hydrophobic Fumed Silica	2.60	1.460	M4	4.172×10^{-21}
Polyethylene glycol	16.13	1.459	M5	2.611×10^{-21}
Ethylene oxide propylene oxide copolymer	6.98	1.580	M6	3.810×10^{-21}

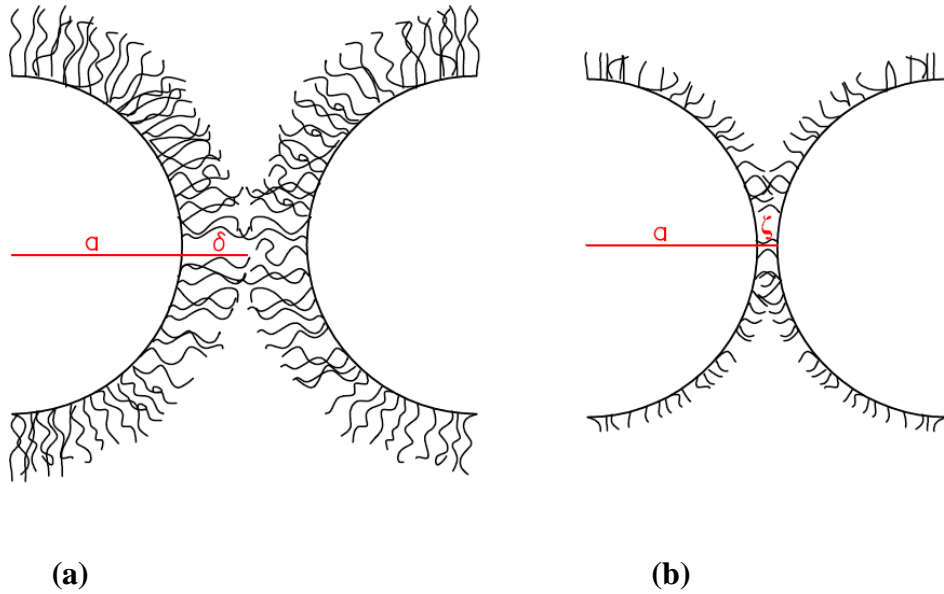


Figure 4.9. Schematic representations for particles with adsorbed layers, **(a)** a high molecular weight polymer is adsorbed on the particle surface, hence forming a dense polymer layer. This situation generates strong repulsive force, **(b)** low molecular weight polymer is adsorbed on the particle surface, thus forming a thin adsorbed polymer layer. This situation generates a weak repulsive force, and consequently vdW attractive force might become dominant.

In suspension M4 (table 3.2), in addition to hydrogen bonding between the surface hydroxyl of silica particles and ethylene oxide portion of the polymer, there are van der Waals interactions between methyl groups of silica particle and propylene oxide portions (figure 4.3.b). Preferential interactions between the polymer and particle favor the shear thickening flow (figure 4.2). However, considering HR of dispersed phase which is measured to be around 200-250 nanometer by dynamic light scattering, one may conclude that there also exists flocculation. According to the previously noted relation $F = A_{eff} \left(a / 12H^2 \right)$, the vdW attraction forces between the particles are linearly proportional to the effective hamaker constant. For that reason the higher value of effective Hamaker constant of M4 (4.172×10^{-21} J, see table 4.3) than M3 ($1,960 \times 10^{-21}$ J, see table 4.3) brings about higher attractive force between particles. This explains why hydrodynamic radius of M4 is bigger than M3. Raghavan et al. states that sols have to be non-flocculated to behave as a shear thickening fluid [44]. In some other relevant works, it was also suggested that for a colloidal suspension

to exhibit shear thinning behavior followed by the shear thickening, it should be a concentrated suspension of non-agglomerating dispersed phase [4, 35]. On the other hand, we have shown that colloids can be shear-thickened without the necessity of having very high particle volume fraction and non-flocculated dispersed phase. Stating more explicitly, although suspensions M3 and M4 have relatively small particle volume fractions ($\phi = 0.11$, calculated from density) and contain small flocculated structures, they thicken.

Modifying surface chemistry of particles and/or the polarity of liquids alter the interactions among the constituents, which leads to the replacement of the shear thickening by thinning or vice versa at high shear rates. For instance, strong attractive particle interactions increase the tendency of the formation of flocculation and/or networks due to the inter-particle linkages in suspension, which results in the formation of a colloidal gel. Hence, colloids with strong attractive particle interactions are in tendency of showing high viscosity at low shear rate, and shear thinning behavior at higher shear rates [4]. In suspensions M5 and M6 hydrogen bonding and/or van der Waals attractive interaction forces exist between particles depending on the dielectric constant, refractive index and polarity of liquid molecules [44]. The existence of these attractive forces induces flocculation in the system, which results in the formation of a colloidal gel.

In suspension M5 (table 3.2), the partially hydrophobic fumed silica particles, which are prepared by replacing the half of the surface hydroxyl with methyl groups, are used as dispersed media. In this system, there are two main types of interactions; namely, particle-particle interactions through methyl groups (promoting flocculation), and particle-oligomer interaction through the surface hydroxyl of silica particles and OH end groups of peg molecules (promoting dispersion) (figure 4.3.c). As a result, the net attractive forces between hydrophobic particles are sufficient to promote the formation of moderate size flocs through coalescence of aggregates whereby M5 colloid exhibits a high zero shear viscosity compared to M3 (figure 4.2). The network structure or larger flocs cannot be formed in this system due to the existence of particle-oligomer interaction. The comparison between the effective Hamaker constant of M3 and M5 (table 4.3) points to higher vdW attraction tendency of particles in M5. The colloid M5 shows shear thinning behavior over a wide range of low shear rates because weak van der Waals interactions among hydrophobic particles can easily be destroyed by shear force, and the entrapped liquid molecules begin to be released into continuous media. Alignment of free oligomer chains in the direction of shear field also

decreases the viscosity at low shear rates as well. Afterward the shear thickening flow is observed over wide range of higher shear rates because small methyl groups are incapable of preventing the particle-oligomer interaction through an effective steric barrier [51].

In the case of the suspension M6 (table 3.2), the hydrophilic fumed silica interparticle linkage corresponding to large flocs structure is formed in ethylene-propylene oxide copolymer which is more non-polar than polyethylene glycol. The observation of very high zero shear viscosity in M6 is attributed to the strong particle-particle hydrogen bonding via silanol (Si-OH) group (figure 4.2 and figure 4.3.d). The lower value of the Hamaker constant of M6 compared to M5 (table 4.3) is also proving that the hydrogen bonding is the main contribution to the particle-particle interaction in M6. One should note that in this system, the hydrogen bonding between particles and the polymer is not favored due to the high molecular weight of the polymer. Strong particle-particle interaction through hydrogen bonding prevents the infusion of long polymer chains into gap between particles, thereby decreasing the possibility of interaction between the particle and the polyethylene oxide portion of the polymer. The higher flocculation tendency of M6 system can be further concluded through examining transmission electron microscopy images as shown in figure 4.10 and dynamic light scattering results presented in figure 4.11.



Figure 4.10. Cryo-TEM image of M6.

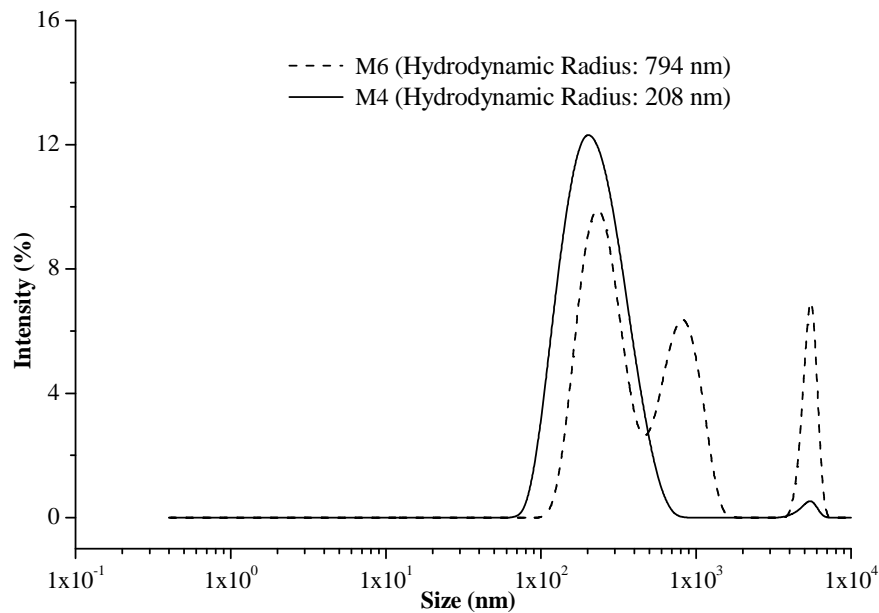


Figure 4.11. DLS results of the M4 and M6 suspensions.

To further elaborate on the shear thickening and thinning behavior of colloidal suspensions, we have compared yield stress values of two selected samples (i.e., M4 and M6, refer to figure 4.12), which might be used as a simple criterion for the existence of shear thickening/thinning [52]. The yield stress of a material is usually defined as the stress below which no flow will occur. Recall that the attractive particle interactions lead to flocculation in suspension, and the network density or floc size depends on the strength of the particle interactions. Yield stress value increases when the floc size is bigger. For instance, M6 includes three dimensional networks (highly flocculated fumed silica particles) due to strong particle-particle interaction, and therefore shows very high yield stress (≈ 25 Pa) as can be seen in figure 4.12. It should be noted that the applied shear stress is to be higher than the yield stress in order to overcome the interaction forces between particles and in turn to destroy the big flocculated structure. Flocculated particles entrap the continuous media within the network. When colloids with network structures are exposed to shear forces, the network can be disrupted whereby relatively smaller size isolated agglomerates form. Consequently, entrapped liquid molecules are released into matrix, which decreases the viscosity of the system, and the colloid shows thinning behavior. Upon the removal of shear force, agglomerates coalesce, thus forming space filling networks reversibly. One can expect

samples M6 can be shear thickened by the breakdown of all agglomerates into aggregates at very high critical shear rate. However, such a high shear rate is not measurable in the current commercial rheometers so these types of suspensions are referred to as shear thinning fluids. As for the M4 suspension, the yield stress is of such a low value that 0.03 Pa stress is adequate to initiate the flow. In this suspension, the shear thickening region starts at 19 Pa, which is significantly lower than yield stress of M6 suspension even though M4 and M6 have the same continuous phase, weight fraction, and nearly the same primary particle size. This rheological dissimilarity in both suspensions (M4, M6) is due to the different surface chemistry of particles. Considering yield stress values of both colloids, one should expect that M4 shows shear thickening due to the affinity of polymer chains towards particle surfaces and the formation of small size flocs which are not linked into a network. On the other hand, M6 exhibits shear thinning owing to highly flocculated and volume filling network systems.

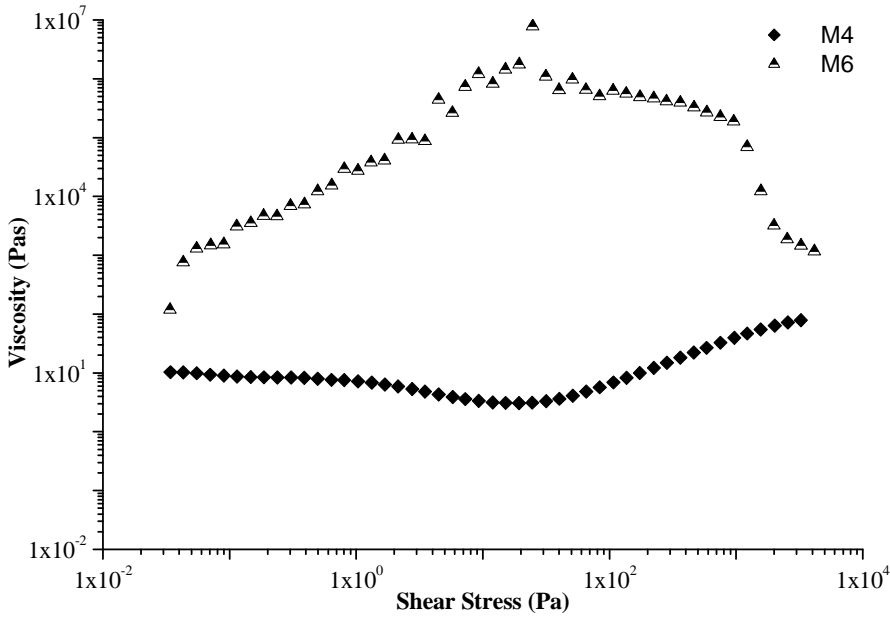


Figure 4.12. The viscosity versus shear stress profile of the M2 and M4 suspensions.

4.1.2.2. Oscillatory shear rheological analysis

The results of dynamic rheological experiments on suspensions M4 and M6 are presented in figure 4.13. The decrease in the elastic modulus with the applied strain implies the existence of flocs in M4 which even though shows shear thickening. This conclusion might be supported by referring to the computational study that employs a coarse-grained “dissipative particle dynamics” model by Raos et al.; it was shown that the elastic modulus of

flocculated colloids decreases over the narrow strain range (0-0.8) [53]. On the other hand, no change in the elastic modulus was reported for dispersed colloids [53]. Furthermore, as concluded from figure 4.13, the colloid M6 (composed of hydrophilic fumed silica and ethylene oxide-propylene oxide copolymer) is of a greater flocculation than M4. It should be noted that despite the fact that both M4 and M6 have the same continuous media, initial particle size, and volume fraction, M6 cannot show the shear thickening behavior unlike M4 due to surface chemistry of particles and concomitant change of particle-particle interaction strength. Depending on the size of the flocs, shear thinning or thickening can be observed in colloids. If the applied shear rate is able to break down the flocculated structures, shear thickening is observed, otherwise shear thinning.

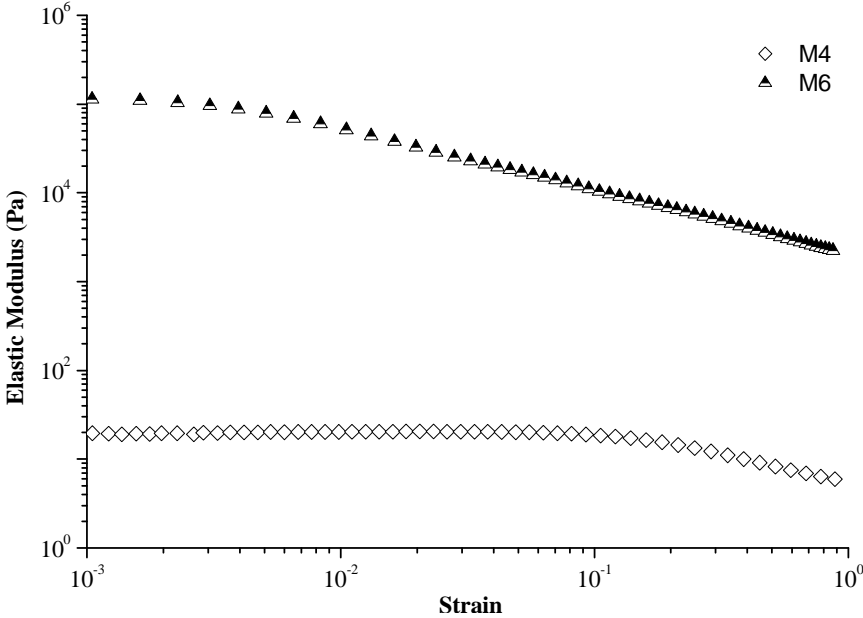


Figure 4.13. Elastic modulus versus strain profile of M2 and M4 suspensions.

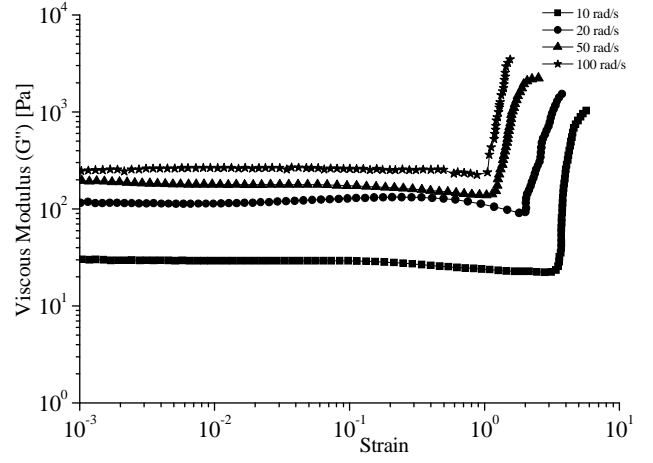
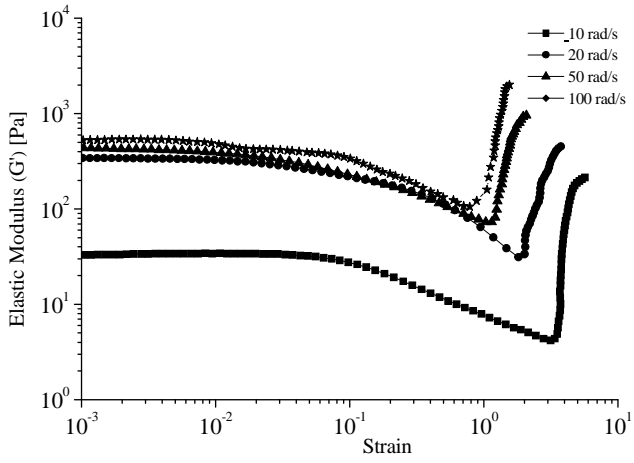
During steady-shear measurements, the viscosity of the sample is measured as a function of the shear stress or shear rate. Therefore, these analyses may not give detailed information about the microstructures present in colloidal systems. To be able to understand the microstructure and its effect on the viscoelastic property of a suspension, we have conducted dynamic oscillatory strain and frequency sweep experiments on different colloids. Oscillatory shearing motion is a common form of flow used to characterize viscoelastic fluids. In dynamic oscillatory experiments, the suspension is usually subjected to a sinusoidal oscillating strain and the resulting stress is measured at various frequencies. During this

experiment, the rheometer records the peak strain applied, the resulting peak stress and the difference between the strain and stress wave forms at each frequency. The stress-strain relation is given by the formula $\sigma = \gamma[G'(\omega)\sin(\omega t) + G''(\omega)\cos(\omega t)]$ where σ , γ , ω , G' and G'' are the stress, the strain amplitude, the frequency, elastic modulus, and viscous modulus, respectively. The stress component in-phase with the deformation defines the *elastic* (or storage) modulus G' which is related to the elastic energy stored in the system on deformation. The component out-of-phase with the strain gives the *viscous* (or loss) modulus G'' which is linked to the viscous dissipation of the energy in a system. Detailed relation between the elastic and viscous modulus with phase angle, complex modulus, and complex viscosity is given by Larson et.al. [54].

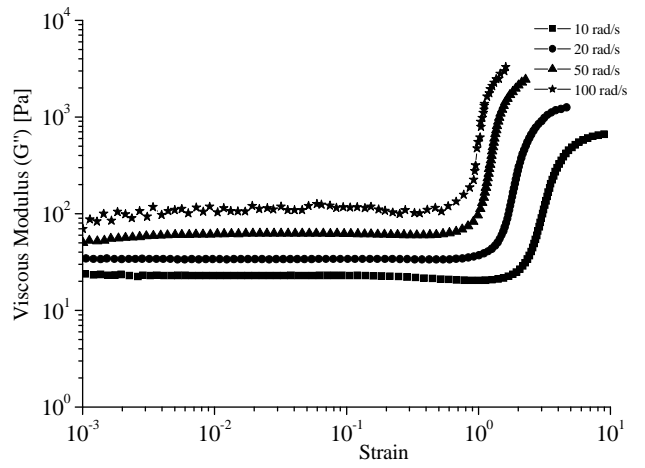
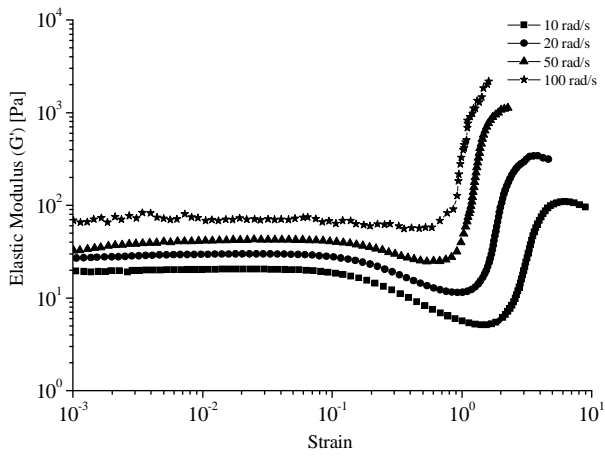
Linear and non-linear rheological responses of complex fluids are of great interest in strain sweep analysis in which the deformation amplitude of tested sample gradually increases at a fixed oscillatory frequency. This constant frequency should be selected such that it must be in the middle of the frequency sweep range. Small amplitude oscillatory shear (SAOS), based on the small amplitude strain imposed and the stress response, gives linear viscoelastic region. Also the onset of nonlinear response is expected at larger amplitudes of oscillatory shear (LAOS) in strain sweep analysis. Conducting the strain sweep test in linear viscoelastic region gives information about the microstructure of the particles within a colloidal suspension at a stationary condition. On the other hand, the non-linear viscoelastic region is crucial to determine the microstructural change of the system under the application of higher forces in order to predict processing behavior of polymer, colloidal system, etc. After the determination of linear and non-linear viscoelastic region, a frequency sweep analysis can be performed. During the frequency sweep test, frequency is increased at constant strain/stress amplitude which is selected from linear or non-linear viscoelastic region of the strain sweep test. If frequency sweep test is performed for the determination of microstructure of the suspension, the selection of strain/stress values from linear region in the strain sweep test is required. The spectrum of the frequency sweep can be separated by three zones; namely, terminal zone, plateau zone (where G' and G'' cross over) and transition zone. The simulations of time dependent shear behavior of suspensions reflect the primary importance of frequency sweep experiment. Short term behavior is simulated by rapid oscillations (at high frequency) and long term behavior is simulated by slow oscillations (at low frequency). In the dynamic oscillatory strain sweep test, the point where G' and G'' increases/decreases abruptly is called

as critical strain while the critical frequency for dynamic oscillatory frequency sweep can be defined as the frequency which correspond to the first crossing point of elastic and viscous modulus. Critical strain/frequency is an important parameter since significant change of microstructure begins to occur at these certain points. In addition, the microstructure of suspensions and intermolecular interactions therein can be distinguished based on the viscoelastic response. For instance, the decrease in G' with the strain amplitude is referred to as the *strain softening* while the increase of G' indicates the *strain hardening* behavior [8]. The increase/decrease in storage modulus at large strains (strain hardening/strain softening) in oscillation experiment corresponds to an increase/decrease in viscosity at high shear rates (shear thickening/shear thinning) in steady shear experiment.

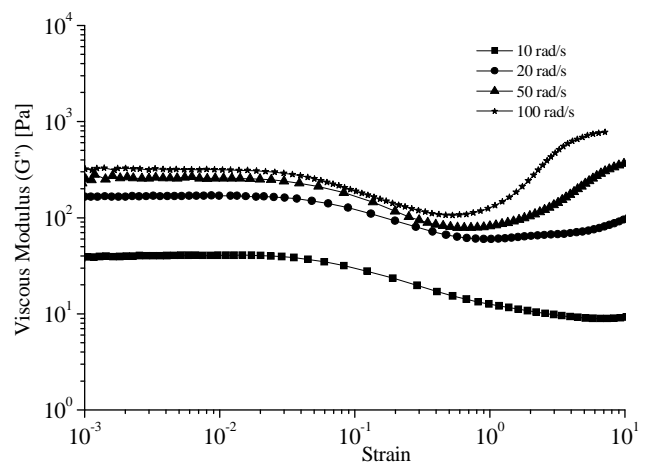
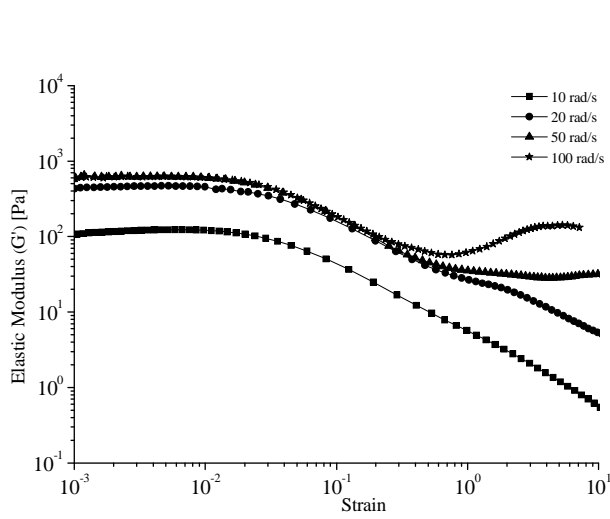
In order to explore the structural rearrangement in colloids under increasing strain/frequency value, in Figure 4.14 are presented the results of strain sweep experiments under oscillatory shear for various colloids, which are plotted as elastic modulus G' and viscous modulus G'' versus the strain amplitude at different constant frequencies. The strain sweep test of the suspension M3 indicates that the critical strain shifts towards smaller value as the frequency of the deformation increases (figure 4.14.a). Nearly constant elastic and viscous modulus at very low strains and the drastic decrease in elastic modulus at higher strain values suggests the existence of flocculated structures in the system. Figure 4.14.a shows that both moduli of suspensions show an increase after a critical strain value. The sharp increase of elastic modulus after the critical strain value indicates strain hardening behavior which is related to the breakdown of internal structures. The breakdown of agglomerated silica particles into aggregates and associated increase in friction among them leads to the increase in viscous modulus due to the higher energy dissipation. Friction between the polymer matrix and particles should be also considered although energy dissipation is mainly controlled by friction between aggregate particles. The dynamic oscillatory frequency sweeps under a constant strain were performed on the suspension M3 using the stress controlled rheometer with a cone geometry (Figure 4.15.a). This test is carried out at high strain amplitude value which is selected from non-linear viscoelastic region. For M3, the long term behavior of suspension is liquid-like since $G' \ll G''$ in terminal zone (at low frequencies) while $G' \gg G''$ in transition zone (at higher frequencies) which indicates that the short term behavior of the suspension is more solid-like. In addition, liquid to solid like transition occurs at a frequency where the complex viscosity begins to increase.



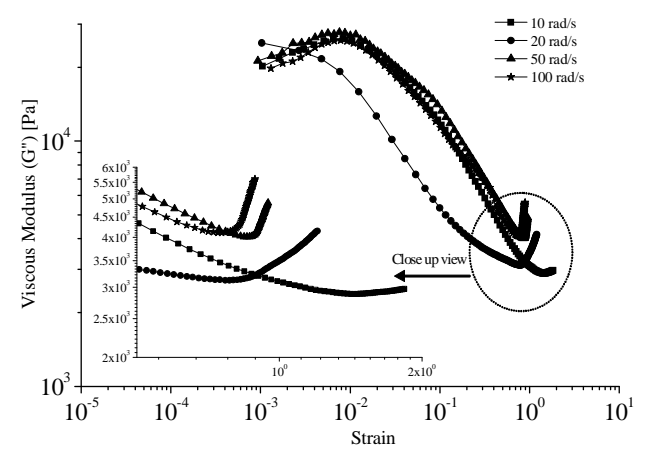
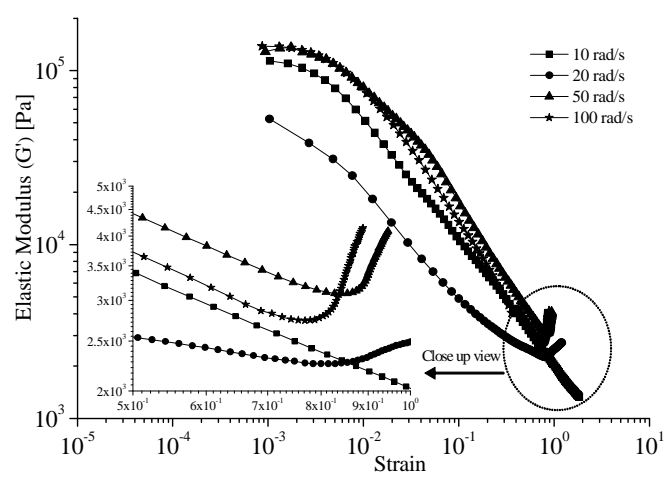
(a)



(b)

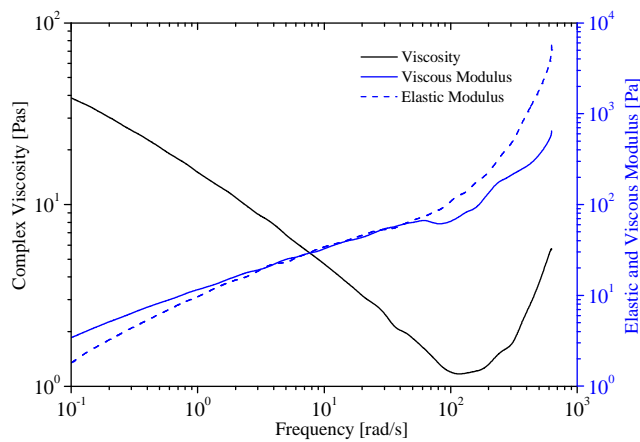


(c)

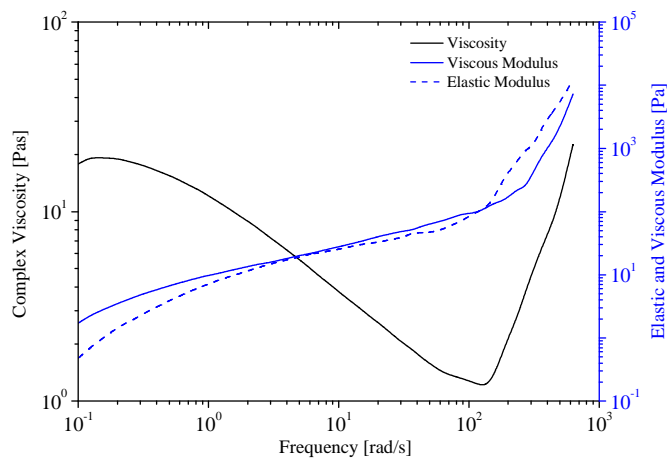


(d)

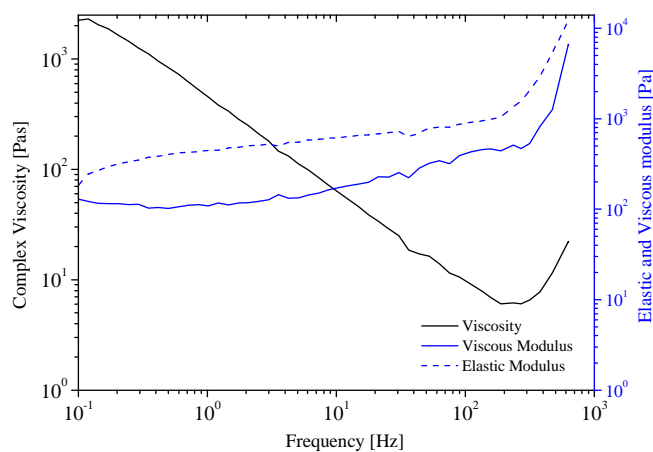
Figure 4.14. Strain sweep experiment under oscillatory shear (a)M3, (b)M4, (c)M5, (d)M6.



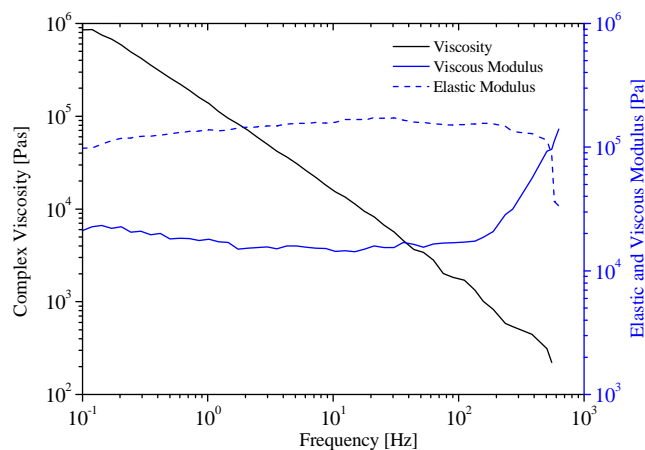
(a)



(b)



(c)



(d)

Figure 4.15. Frequency sweep analysis at 0.1 strain amplitude; (a)M3, (b)M4, (c)M5, (d)M6

As can be seen from Figure 4.14.b, the colloid M4 shows a similar viscoelastic behavior to M3 where G' and G'' are constant at very low strains, and G' exhibits a rapid decrease at higher strain values. Both storage and loss moduli of M4 show a rapid increase at a critical strain under the oscillatory shear. In the strain sweep test of M4, the critical strain also decreases with increasing frequency while the degree of strain hardening increases. Figure 4.15.b. shows the frequency dependence of elastic and viscous modulus at 0.1 strain amplitude. At low frequencies, the value of G'' is greater than that of G' , which implies that

the energy dissipated E_d by viscous forces is larger than that stored within the structure of the suspension. Otherwise stated, at low frequencies, the suspension M4 mainly possesses a viscous property thereby behaving liquid-like. After reaching the minimum value of complex viscosity, the rate of increase of elastic modulus is faster than viscous modulus. This behavior shows that the transition from viscous to elastic had taken place. Therefore, the crossover of G'' and G' at critical frequency (ω_c) in oscillatory shearing corresponds to critical shear rate where transition from liquid-like behavior to solid-like behavior is observed in steady shear experiment. Recall that the values of storage modulus G' represent the intensity of elasticity and the change of elastic modulus can be associated with the structural changes from flocs to aggregated structure. Hence, the suspension M4 shows more solid like character at high frequency.

Figure 4.14.c shows the oscillatory shear result of M5 from which one can clearly notice that G' and G'' of M5 are not dependent on the strain amplitude at very low strain values while they are strongly dependent on the strain amplitude at higher strain values. Unlike M3 and M4 which show strain hardening behavior, both G' and G'' decreases over the whole range of the strain sweep at low frequency (e.g. 10 rad/s), which indicates the long term behavior of the fluid. The drops in storage modulus unlike M3 and M4 over the whole range of strain points to the existence of moderate size of floc in the colloid. At higher values of frequency (i.e., 20, 50, 100 rad/s), suspensions show strain hardening, which is nonetheless not as strong as those in M3 and M4 owing to the existence of moderate size flocculated structures. Figure 4.15.c shows the angular frequency dependence of G' and G'' for M5 at a constant strain value. Both G' and G'' exhibit very weaker dependence on frequency than M3 and M4. Reason behind this weaker frequency dependence of M5 can be explained by attractive interparticle interaction between disperse phases which are strong enough to develop more rigid and bigger size flocs. These bigger size flocs are more resistance to motion under applied stress. One can also note that $G' > G''$, which suggests the formation of gelation due to the particle interaction.

As seen from Figure 4.14.d, the strain sweep of M6 shows similar behavior to M5 at the frequency range of 10-20 rad/s in terms of the fact that the elastic modulus decreases over the whole ranges of strain. It is known that the modulus of strongly flocculated gels tends to be highly-strain dependent as in the case of M6. Furthermore, it was shown by Larson et.al. that the strain sensitivity increases when the flocculation becomes stronger since the strongly

flocculated gels are likely to be more brittle than weakly flocculated ones [60]. As a result, both moduli of M6 show variation even at very low strain amplitude unlike M5 which might be considered as an evidence for the existence of the highly flocculated/network structure in a given system. It is important to point out that M6 shows only shear thinning behavior in steady shear experiment while the same suspension shows strain hardening in oscillatory shear experiments with a strain sweep mode especially at higher frequency values which simulates short term behavior of suspension (see, Figure 4.14.d). Barnes et. al. in their review article concluded that all dispersions might exhibit shear thickening behavior under the right conditions [4]. Therefore, we think that the colloid M6 can also be shear thickened at very high critical shear rate. However, such a high shear rate is not measurable in the current commercial rheometers so this type of suspensions is in point of fact called as shear thinning fluids. In the terminal and plateau zones of frequency sweep (Figure 4.15.d), M6 also shows little frequency dependence, and G' is greater than G'' , which is a similar behavior to M5.

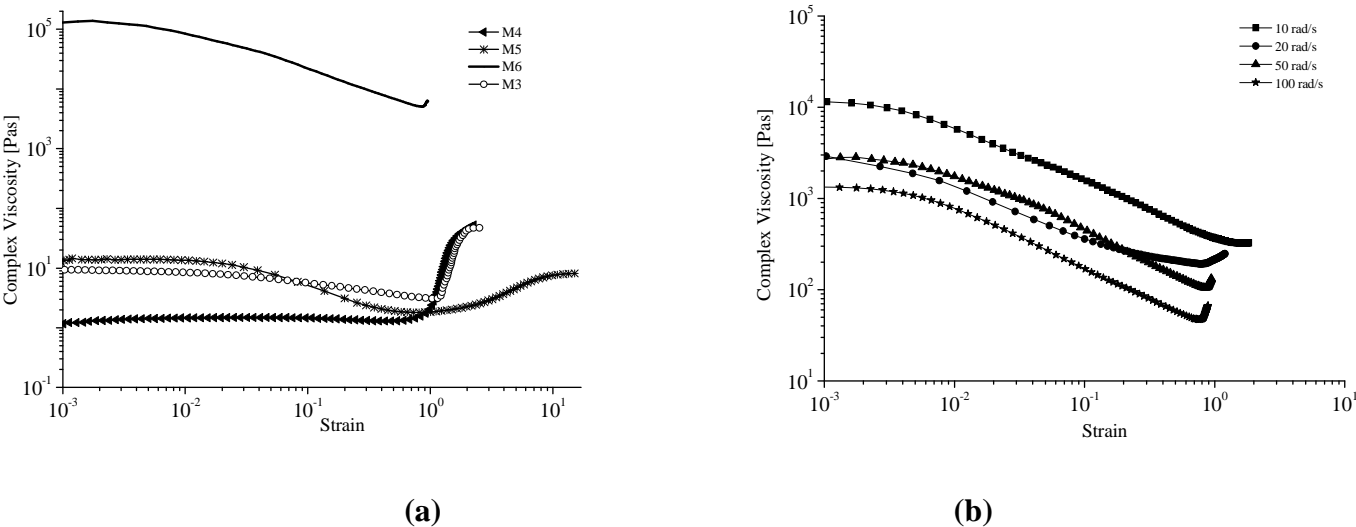


Figure 4.16. (a) Complex viscosity of suspensions at frequency 50 rad/s during strain sweep analysis and (b) Complex viscosity of M6 at different frequencies.

Figure 4.16.a presents complex viscosity versus strain plots for suspensions (M3, M4, M5 and M6). These suspensions exhibit strain hardening at high strain amplitudes (at frequency 50 rad/s) since their complex viscosity shows an abrupt jump to higher levels at particular strains. The graphs further denote that the complex viscosity of these suspensions

was initially independent of strain at low strain amplitudes, then obvious decrease in complex viscosity occurs, and finally dramatic strain hardening takes place, which is followed by the jump of complex viscosities to higher values after reaching the minimum viscosity level. The change in the viscosity of the silica suspensions as a function of strain is prudently attributed to the microstructural change in these colloids. More clearly, at small strain amplitude, Brownian motion and the interparticle forces are able to restore the structure to the equilibrium state during the oscillatory shear; therefore the viscosity almost remains unchanged. As the strain increases further, the relaxation and the alignment of the molecular chain of the PEG contributes to the decrease in the viscosity in the thinning regime. At the critical point, the structural breakdown induced by the very high strain amplitudes becomes significant and the Brownian motion and the interparticle forces are no longer capable of restoring the microstructure, thus the viscosity increases. Figure 4.16.b present plots complex viscosity versus strain for M6 at 4 different constant frequencies. At low strain values, the initial complex viscosities of suspensions decrease with increasing frequency amplitude due to the breakdown of network structure. In essence, the application of 100 rad/s frequency causes the formation of smaller agglomerate structure than 50 rad/s thereby enabling the entrapped liquid molecules to be released into the continuous media and consecutively leading to decrease in the initial complex viscosity. For all frequency values, the complex viscosity keeps decreasing until reaching the critical strain. After the critical strain values, the strain hardening behavior can be observed for the frequency of 20, 50, 100 rad/s whereas the complex viscosity is constant at 10 rad/s. This is an expected result since the application of higher frequency on a suspension can break down agglomerate structure to aggregates much more easily.

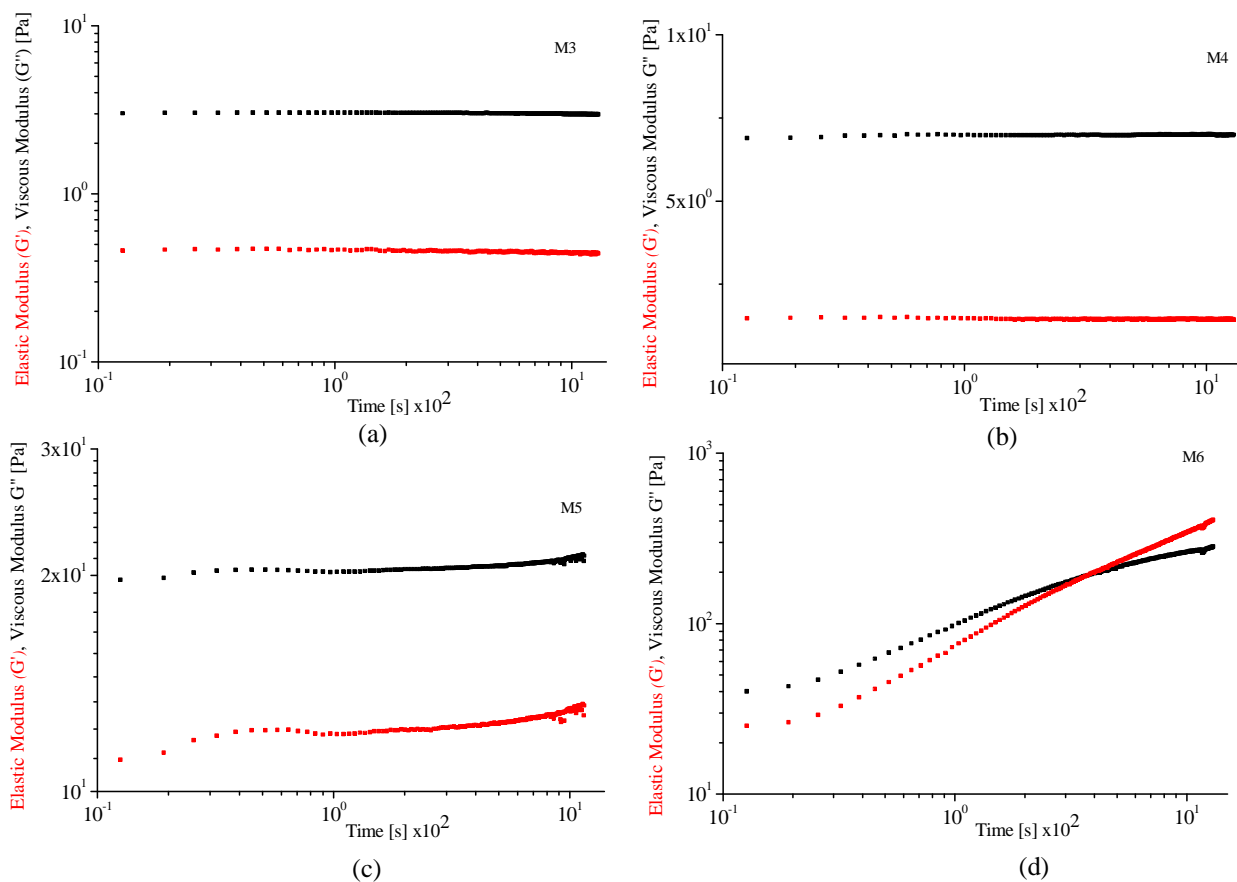
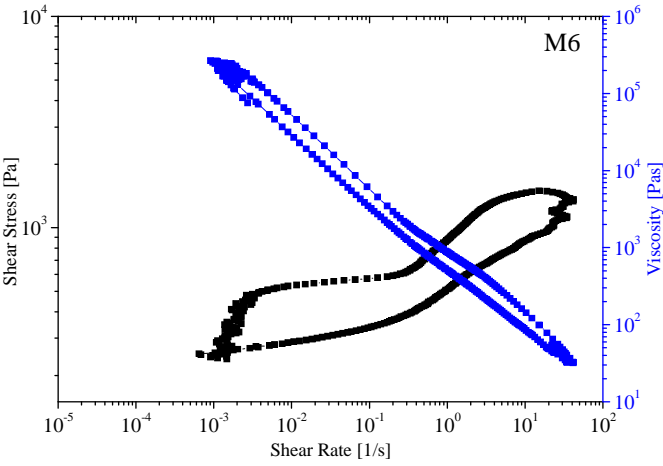


Figure 4.17. Single frequency (1.59 Hz) oscillator shear experiments (at controlled stress (10 Pa)) (a) M3, (b) M4, (c) M5 and (d) M6.

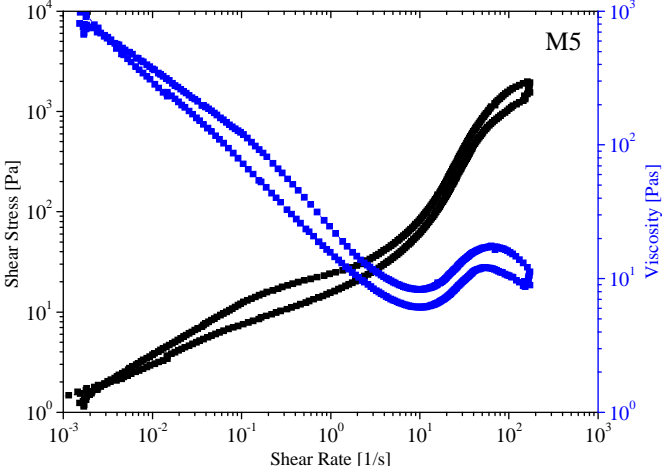
In order to examine the flocculation rate of particles within different continuous media, high pre-shearing with a shear rate of 1000 s^{-1} is applied on colloids in order to break down all microstructures and then single frequency (1.59 Hz) oscillatory shear at controlled stress (10 Pa) was performed to determine the ability of given suspension to recover the microstructure. Figures 4.17.a and 4.17.b show that the elastic moduli of suspensions M3 and M4 do not change with respect to time, which means that these structures slowly reform when the shearing force is removed. On the other hand, M5 shows more rapid increase in modulus in comparison to M3 although the liquid phase of both suspensions is the same. The rapid increase in modulus proves the existence of particle-particle interaction through attractive van der Waals interaction in the system. Finally, for the suspension M6, it is clearly seen from Figure 4.17.d that the elastic modulus becomes greater than the viscous modulus after their

cross over, which suggests that there exists strong particle-particle interaction and hence tendency for the formation interparticle linkage in M6.

Figure 4.18 shows the hysteresis behavior of viscosity during the cycles of increasing and decreasing shear rate. Flow curve is obtained in a single experiment in which the shear rate is steadily increased at a constant rate from zero to some maximum value and then decreased at the same rate to zero whereby the hysteresis loop is formed. The area between the shear stress versus strain loop gives magnitude of thixotropy. Thixotropy is associated with the rate of structure breaking (disruption) in the material when stress is increasing and the buildup of structure with decreasing stress. The flow curves of the shear stress versus strain (seen in Figure 4.18) and calculation of area of all samples (M3, M4, M5, M6) display the thixotropic behavior (see Table 4.4). Results of analysis indicate that thixotropy is higher in shear thinning fluids because attractive interactions between particles cause development of big flocculated structures which show higher structural break down with increasing shear rate and faster buildup of microstructure with decreasing shear rate.



(a)



(b)

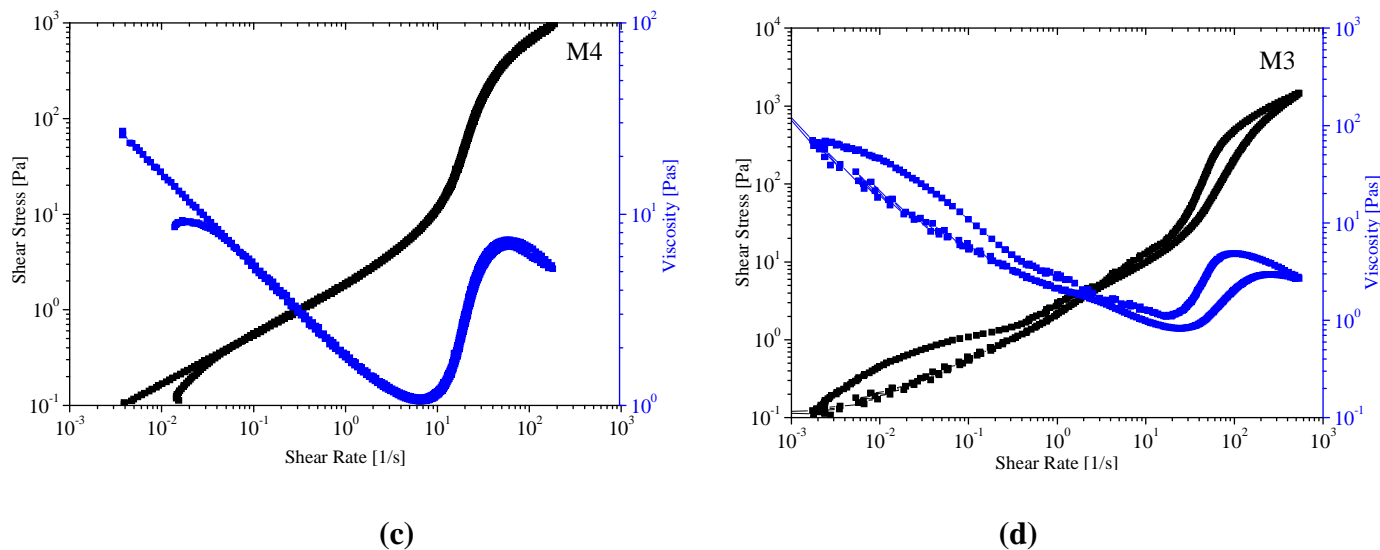


Figure 4.18. Thixotropic analysis (preshear is applied at 5 Pa); **(a)** HFSi (10 wt%) and PEO-PPO, **(b)** HPFSi (10 wt%) and Peg, **(c)** HPFSi (10 wt%) and PEO-PPO and **(d)** HFSi (10 wt%) and Peg.

Table 4.4. Results of quantitative thixotropic analysis.

Suspensions	Area Calculation Results
HFSi (10 wt%) and PEO-PPO	2995.5
HPFSi (10 wt%) and PEO-PPO	84.52
HPFSi (10 wt%) and Peg	773.55
HFSi (10 wt%) and Peg	544.5

4.2. Physical Parameters

To examine the effect of molecular weight on the degree of shear thickening, we have studied M3, M7, M8 and M9 suspensions (table 3.2). To be more specific, in M3, the difference between the minimum and the maximum viscosity is 8.63 Pas at the critical shear rate, while in M9, it is 245.24 Pas (see, figure 4.19 & 4.20). Polymers with a high molecular weight will result in an increased adsorbed layer thickness. Therefore, the hydrodynamic

radius of particles in different molecular weight oligomer increases due to the longer oligomer chains (see, figure 4.23). On the other hand, bigger floc structures, which exist in high molecular weight continuous media, composed of smaller number of bounded aggregate. The adsorption of longer oligomer chains on particles creates stronger steric forces and the attractive interactions between particles are therefore weakened. As a consequence, shear rate value at which thickening transition is first observed decreases when the molecular weight is increased from 200 to 600 because it is easier to break flocs which are composed of smaller number of weakly bounded aggregate. In addition, critical shear rates for M3, M7, M8 and M9 suspensions are measured to be 82.10, 34.71, 22.80, and 10.80, respectively, see figure 4.20.

The effects of particle size, mass fraction and preprocessing condition on the shear thickening behavior were also studied within the context of the current work. The experimental results indicate that there is a distinct rheological difference between suspensions M12 and M3 although both suspensions are composed of the same constituents with the identical weight fractions. The fact that M12 mixture shows a Newtonian fluid behavior in the viscosity profile (see, Figure 4.21) is attributed to the greater particle size and the concomitant decrease in the surface area of the dispersed media. The effect of the weight fraction on the shear thickening can be clarified through comparing the rheological behavior of suspensions M3, M10, M11. From Figure 4.22, one can deduce that particles shows higher zero shear viscosity due to higher flocculation tendency with the increased particle concentration (see figure 4.23). Although bigger floc structures exist in the suspension, shear thickening responses of M10 and M11 are enhanced by the increase in the particle weight percent (see, Figure 4.22). It is known in the literature that the critical shear rate is linearly dependent on the interparticle distance and has an inverse linear dependence on the surface area [8]. Hence, the greater the weight percent and/or volume fraction, the lower is the value of the critical shear rate [39, 54], which is in very good agreement with our observations as well. Preprocessing speed (mixing speed) is one of the parameters that also have an effect on shear thickening behavior. In Figure 4.24 are given the viscosity profile for suspensions M8 (preprocessed at 5000 rpm) and M13 (preprocessed at 11000 rpm). The M13 suspension shows significantly larger increase in viscosity (i.e., 248.04 Pas) at the critical shear rate than M8 (i.e.. 80.95 Pas). This is a quite expected result since the higher mixing speed improves the dispersion of particles. The HR for M13 was measured to be 210 nm, while for M8, it is

262 nm. The decrease in HR of particles leads to an increase in the total surface area of silica particles. As a conclusion, it should be stated that the critical shear rate decreases when the suspension is preprocessed at a higher mixing rate.

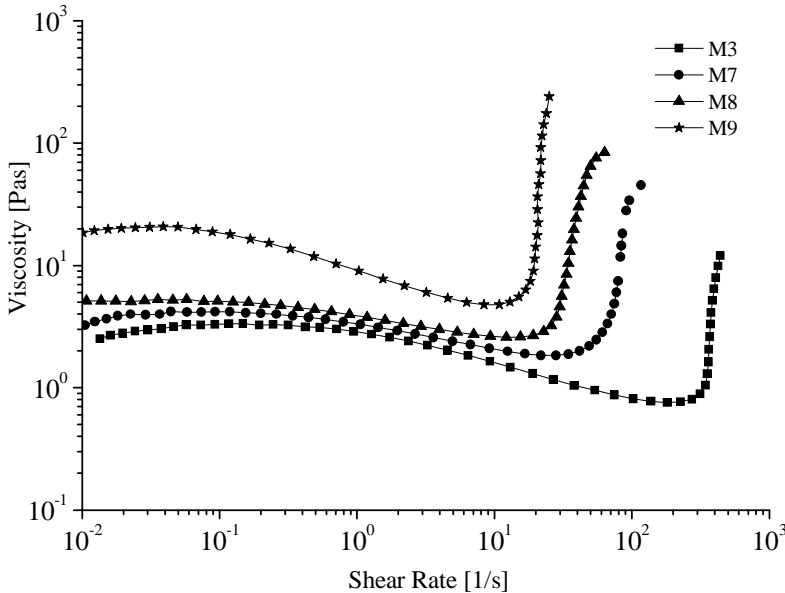


Figure 4.19. Steady shear experiment of suspensions composed of different molecular weight oligomeric matrix

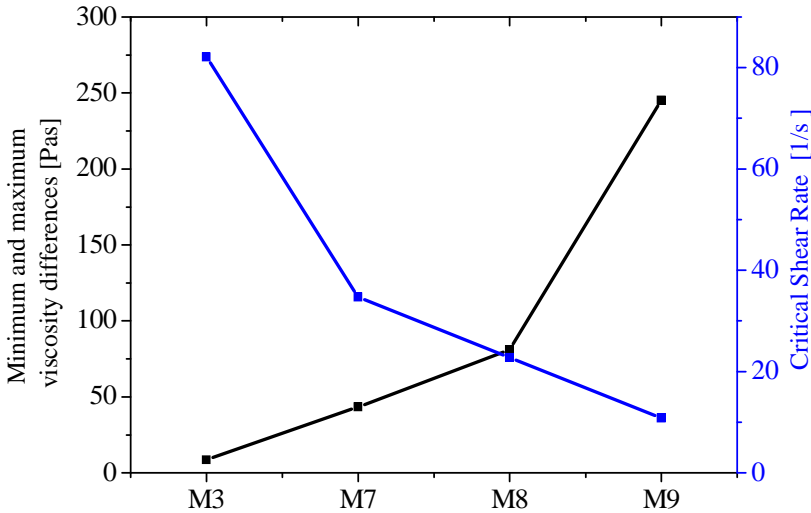


Figure 4.20. Minimum and maximum viscosity differences and the critical shear rates for suspensions (M3, M7-M9)

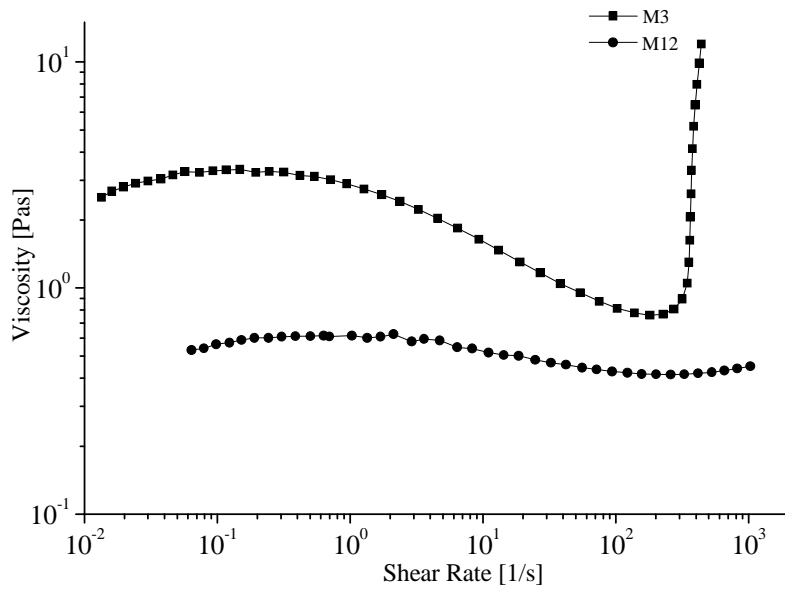


Figure 4.21. Steady shear viscosity profile of suspensions composed of different sizes particles

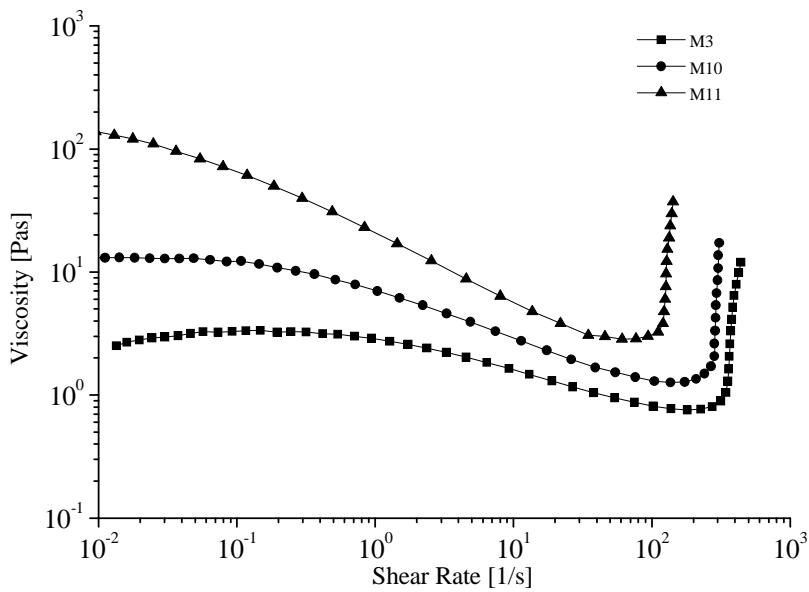


Figure 4.22. The effect of particle mass fraction on the non-Newtonian flow behavior

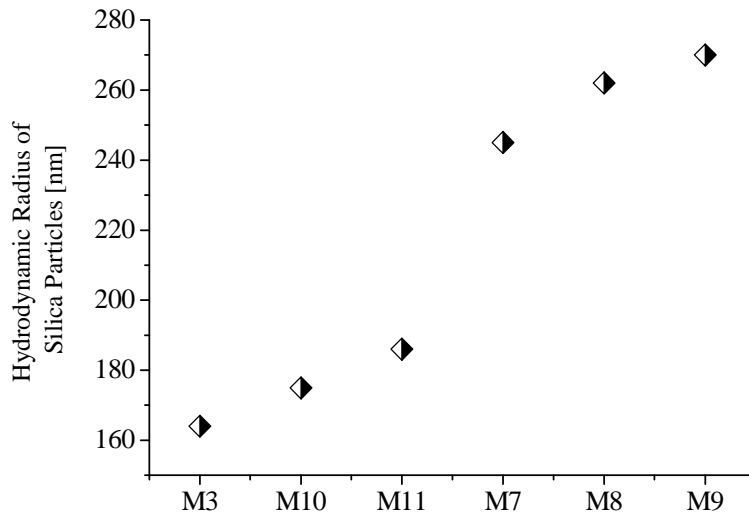


Figure 4.23. Hydrodynamic radius of particles in suspensions measured by dynamic light scattering of suspensions

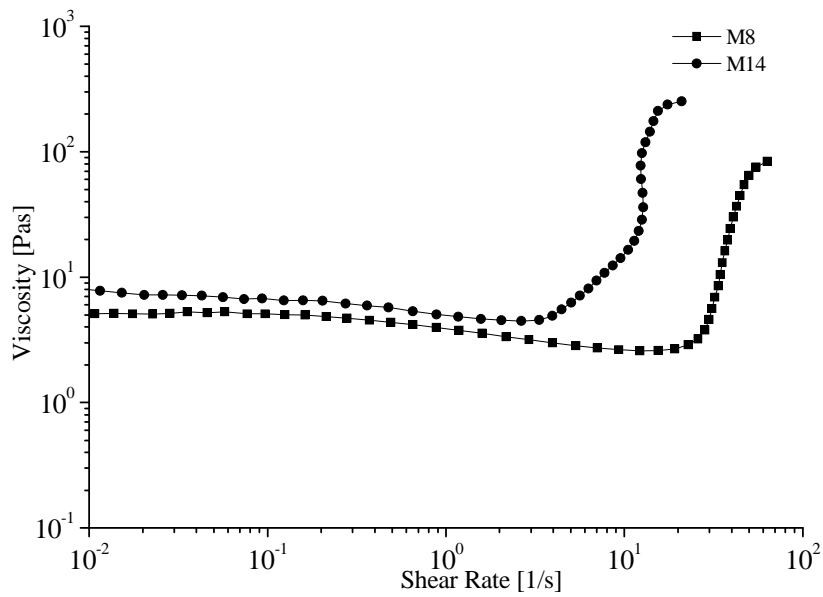


Figure 4.24. Effect of preprocessing speed on the dispersion and concomitant change of rheology of the suspensions

CHAPTER V

5. CONCLUSION

The flow curve of polymeric colloids integrated with nano- or micro sized particles shows generally non-Newtonian flow behavior (shear thickening or thinning) under shear. In relevant literature, the shear thickening flow behavior in concentrated, monodisperse and spherical systems has been scrutinized both experimentally and numerically in order to understand the underlying mechanisms. In view of these studies, two well known theories have been proposed; namely, order disorder transition and hydrocluster theories. However, the origin of shear thickening responses of low volume fraction, anisotropic and flocculated systems has yet remained unclear and hence needs to be explained on the basis of other additional physical mechanisms. In this regard, physicochemical control parameters has been investigated in order to understand the origin of the shear thickening behavior of low particle volume fraction, and anisotropic and flocculated systems. To be able to understand these mechanisms, we have experimentally studied the rheology of CNS through measuring their viscosity and electrical resistance under various shear forces together with utilizing several relevant characterization methods.

Result of steady shear rheological analysis give information about the effect of physicochemical parameters on the flow behavior of CNS. Shear thickening behavior is mainly controlled by particle size and mass fraction, surface chemistry of particle, type of continuous phase, and molecular weight of oligomeric liquid phase and preprocessing speed. Firstly, shear thickening behavior of suspensions that are composed of hydrophilic fumed silica and monomeric / oligomeric liquid phase has been studied to understand effect of the continuous phase. It was concluded that higher hydrogen bonding capability of monomeric liquid phase provide better performance but the optimal performance was obtained when oligomeric liquid phase was used. STF samples were prepared by dispersing nanosized silica particles in a different molecular weight of polyethylene glycol (Mw: 200, 300, 400, 600 g/mol) as well, the shear thickening phenomenon is more obvious when the molecular weight is 600 g/mol. Suspensions with three different mass fractions (20 wt%, 25 wt%, 30 wt%) has been studied and it is obvious that extent of shear thickening increase with mass fractions due to higher surface area. At the same mass fraction, suspensions prepared with 2 micron silica particles show Newtonian behavior while 7-40 nm particles point out shear thickening

properties due to higher surface area. In addition to this, preparation of STF sample at higher preprocessing speed provides better dispersion and lower critical shear rate. In addition to steady rheological analysis, dynamic rheological analysis performed in order to understand microstructural change under shear.

The relation between the interparticle interaction and the non-Newtonian flow behavior has been also identified. The suspensions studied are chosen such that constituents have different interparticle interaction strength among themselves since the main focus of this study is to reveal the effects of interaction forces among particle-particle and particles-polymers/oligomer on the rheology. In our colloids, two main interfacial forces were considered; namely, the attractive van der Waals forces, and the repulsive steric forces. Theoretical bases of these forces and their effects on the rheology of low volume fraction, anisotropic, and flocculated systems have been discussed in detail through considering the particle-particle and the particle-polymer/oligomer interactions. At rest, a weak steric repulsion exists through particle-oligomer interaction, but small floc structures form due to the existence of vdW attraction forces in shear thickening suspensions, whereas a strong particle-particle interaction creates very large flocculated structures in shear thinning systems. Our experimental results suggest that the rheology of the suspensions are strongly affected by microstructures developed within colloids under the combined effects of interaction forces among constituents and shear induced mechanical and hydrodynamical forces. To be specific, the high shear force applied on a flocculated colloid break down flocs into small aggregates so that the total surface area of particles increases whereby the viscosity of the colloid increases due to the combinations of several possible reasons. Namely, the friction among particles is expected to be higher when particles are finely dispersed. Additionally, well dispersed particles may act as an array of solid obstacles for the motion of polymer chains. Most importantly, finer particle distribution will increase the likelihood of chemical interactions among constituents thereby leading to a raise in the effective volume fraction of particles, which hinders the motion of polymeric chains. All these points in essence contribute to the development microstructures where the mobility of polymeric chains is reduced. Consequently, the net observable result is the increase in the viscosity of the system. In most of the published relevant literature, it has been stated that for a mixture to show a shear thickening behavior, it should contain high volume fraction, non-flocculated and spherical particles, and the shear thickening behavior of such mixtures has been explained through

order-disorder and hydrodynamic clustering theories. On the contrary, it is in this work shown that suspensions composed of low volume fraction, flocculated, fractal particles and polymeric continuous media can also display shear thickening behavior, which makes such a system a potential candidate for applications requiring shear thickening materials such as a low weight liquid armor.

APPENDIX

The appendix section of the thesis is structured as follow. In section A.1, investigation of polymer-particle interactions with thermo-gravimetry and atomic force microscopy analysis have been described.

A.1. Investigation of Polymer-Particle Interactions with Thermo-gravimetry and Atomic Force Microscopy Analysis

The polymer-particle interaction in suspensions can be further supported by thermo-gravimetric analysis and atomic force microscopy. In thermo-gravimetric analysis, suspensions M3-M6 were centrifuge for 5 hour and particle with adsorbed polymers precipitated. Then particles with adsorbed polymers in precipitated mixtures were burn at 800 °C in nitrogen atmosphere and residual mass that indicate amount of silica particle in the mixture were determined (see Table A.1). Residual mass of M3 is smaller than M5 as you can see from the thermo-gravimetric analysis results. This conclusion support rheological observations which indicate the existence of stronger polymer-particle interaction in M3 system. Comparison between the residual mass of M4 and M6 reveals that residual mass of M4 is higher than M6 although polymer adsorption on particles is higher in M4. During thermo-gravimetric analysis; in M4, only adsorbed polymers whereas in M6, entrapped polymer molecules within the big flocculated structure were burn. In conclusion, this study exhibit that amount of entrapped polymer molecules in M6 is higher than adsorbed polymer in M4.

Table A.1 STA results of suspension M1-M4

Sample Name	Residual Mass %
M3	18.34

Atomic force microscopy is another important method for studying polymer adhesion on surface as well as their intermolecular interactions. During analysis polymer is stretch between a substrate surface and a cantilever. Figure A.1 shows the adhesion result of M4 and M6 that obtained from AFM measurement. According to results, adhesion of M4 is higher than M6 since more polymer cover the particle surface due to higher polymer particle interaction in M4.

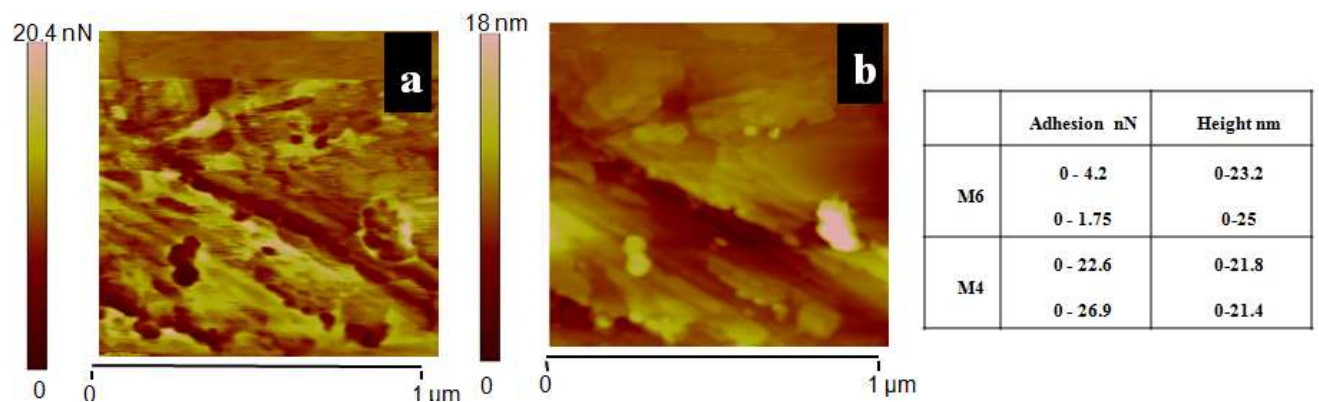


Figure A.1. AFM image of shear thickening fluid **a.** Adhesion image, **b.** Height image

REFERENCES

- [1] Croce, F., Persi, L., Ronci, F., Scrosati, B. *Solid State Ionics* **2000**, 135, 47–52.
- [2] Croce, F., Appetecchi, G. B., Persi, L., Scrosati, B. *NATURE* **1998**, 394.
- [3] Eesa, M., Barigou, M. *Chemical Engineering Science* **2009**, 64, 322 – 333.
- [4] Barnes, H. A. *J. Rheol.* **1989**, 33, 329-366.
- [5] Lee, Y.S., Wetzel, E.D., Wagner, N.J. *J. Mater. Sci.* **2003**, 38, 2825 – 2833.
- [6] Hoffmann, R.L. *J. Rheol.*, **1998**, 42, 111-123.
- [7] Hoffmann, R.L. *J. Colloid Interface Sci.* **1972**, 16, 155–173.
- [8] Boersma, W.H., Laven, J., Stein, H. N., *AICHE J.* **1990**, 36, 321-332.
- [9] Foss, D.R., Brady, J.F. *J. Fluid Mech.* **2000**, 407, 167-200.
- [10] Maranzano, B.J., Wagner, N.J. *J. Rheol.* **2001**, 45 , 1205–1222.
- [11] Laun, R.H.M., Bung, R., Hess, S., Loose, W., Hess, O., Hahn, K., Hadicke, E., Hingmann, R., Schmidt, F., Lindner, P. *J. Rheol.* **1992**, 36, 743.
- [12] Bossis, G., Brady, J.F. *J. Chem. Phys.* **1989**, 91, 1866–1874.
- [13] Raghavan, S. R., Khan, S. A. *J. Colloid Interface Sci.* **1997**, 185, 57-67.
- [14] Negi, A. S., Osuji, C. O. *Rheol. Acta* **2009**, 48, 871-881.
- [15] Osuji, C.O., Kim, C., Weitz D.A., *Phys. Rev. E77* **2008**, 060402.
- [16] Han, C. D., *Rheology and Processing of Polymeric Materials, Volume 1 Polymer Rheology* **2007**, Oxford University Pres, New York.
- [17] Agarwal, P.K., Bagley, E.G., Hill, C.R. *Polym. Eng. Sci.* **1978**, 18-282.
- [18] White, J.L., Tanaka H. *J. Non-Newtonian Fluid Mech.* **1981**, 8-1.
- [19] Fujima, M., Kwasaki, Y., *Rheol. J.* **1989**, 17-60.
- [20] Vinogradov, G.A., Malkin, A.Y., Plotnikova, E.P., Sabsai, O.Y., Nikolayeva, N.E. *Intern. J. Polym. Mater.* **1972**, 2-1.
- [21] Dreval, V.E., Borisenkova, E.K., *Rheol. Acta* **1993**, 32-337.
- [22] Rong, S.D., Chaffey, C.E. *Rheol. Acta.* **1988a**, 27-179.

- [23] Lin, L., Masuda, T., *Rheol. J.* **1990**, 18-190.
- [24] Minagawa, N., White, J.L., *J. Appl. Polym. Sci.* **1976**, 20-501.
- [25] Tanaka, H., White, J.L., *Polym. Eng. Sci.* **1980**, 20-949.
- [26] Markovic, M.C., Choudhury, N.R., Dimopoulos, M., Matisons, J.G., Dutta, N.K., Bhattacharya, A.K. *Polym. Eng. Sci.* **2000**, 40-1065.
- [27] Rong, S.D., Chaffey, C.E. *Rheol. Acta.* **1988b**, 27-186.
- [28] Han, C.D. *J. Appl. Polym. Sci.* **1974**, 18-821.
- [29] Lin, L., Masuda, T., *Rheol. J.* **1989**, 17-145.
- [30] Suetsugu, Y., White, J.L. *J. Appl. Polym. Sci.* **1983**, 28-1481.
- [31] Lobe, V.M., White, J.L. *Polym. Eng. Sci.* **1979**, 19-617.
- [32] Faulkner, D.L., Schmidt, L.R. *Polym. Eng. Sci.* **1977**, 17-657.
- [33] Ertong, S., Eggers, H., Schümmer, P. *Rubber. Chem. Technol.* **1994**, 67-207.
- [34] White, J.L., Crowder, J.W. *J. Appl. Polym. Sci.* **1974**, 18-1013.
- [35] Bertrand, E., Bibette, J., and Schmitt, V., *The American Physical Society* **2002**, 66, 060401.
- [36] Lootens, D., Damme, H. V., He´mar, Y., He´braud, P., *The American Physical Society.* **2005**, 95, 268-302.
- [37] Wetzal, E.D., Lee, Y.S., Egres, R. G., Kirkwood, K. M., Kirkwood, J. E. and Wagner, N. J., *NUMIFORM* **2004**.
- [38] Harzallah, O. A., Dupuis, D., *Springer-Verlag* **2003**, 42, 10–19.
- [39] Raghavan, S. R., Walls, H. J., Khan, S.A., *American Chemical Society* **2000**, 16, 7920-7930.
- [40] Gavin, H. P., Alhan, C. and Oka, N., *J. Struct. Eng.* **2003**, 129, 922–32.
- [41] Ruangrassamee, A., Srisamai, W., and Lukkunaprasit., P., *Struct. Control Health Monit.* **2006**, 13, 809–22.
- [42] Fischer, C., Plummer, J. G., Michaud, V., Bourban, P. E., Manson, J.-A. E., *Springer*, **2007**, 46, 1099-1108.

- [43] Rosen, B. A., Nam Laufer, C. H., Kalman, D. P., Wetzel, E. D., Wagner, N. J., *Proceedings of SAMPE* **2007**. Baltimore, MD.
- [44] Houghton, J. M., Schiffman, B. A., Kalman, D. P., Wetzel, E. D., Wagner, *Proceedings of SAMPE* **2007**. Baltimore, MD.
- [45] Kalman, D. P. , Merrill R.L., Wagner, N.J., Wetzel, E. D., *Applied Materials and Interface* **2009**, 11, 2602-2612.
- [46] Everett, D.H. *Basics Principles of Colloid Science* **1988**, Royal Society of Chemistry: London.
- [47] Israelachvili, J. *Intermolecular and Surface Forces* **1991**, 2nd ed.; Academic Press: San Diego.
- [48] Chhabra, R.P., Richardson, J.F. *Non-Newtonian Flow in the Process Industries, Fundamentals and Engineering Applications* **1999**, Butterworth-Heinemann.
- [49] Goodwin, J., *Colloids and Interfaces with Surfactants and Polymer*, 2nd ed. **2007**; Wiley: Oregon.
- [50] Morrison, I. D. *Colloids Surf.* **1993**, 71, 1.
- [51] Raghavan, S.R., Hou, J., Baker, G.L., Khan, S.A. *Langmuir* **2000**, 16, 1066-1077.
- [52] Brown, E., Forman, N. A., Orellana, C. S., Zhang, H., Maynor, B.W., Betts, D.E., DeSimone, J.M., Jaeger, H. M. *Nat. Mater.* **2010**, 9, 220 – 224.
- [53] Raos, G., Moreno, M., Elli, S., *Macromolecules* **2006**, 39, 6744-6751.
- [54] Larson, Ronald G. *The Structure and Rheology of Complex Fluids* **1999**, Oxford University Press: New York.